THE DETERMINATION OF THE FUNCTIONAL FATIGUE LIFE OF HIGH TEMPERATURE SHAPE MEMORY ALLOYS AFTER COLD ROLLING PROCESS

YÜKSEK SICAKLIK ŞEKİL HAFIZALI ALAŞIMLARIN SOĞUK HADDELEME İŞLEMİ SONRASI FOKSİYONEL YORULMA ÖMÜRLERİNİN TAYİNİ

MUSTAFA SEFA VELİPAŞAOĞLU

DOÇ. DR. BENAT KOÇKAR

Supervisor

Submitted to

Graduate School of Science and Engineering of Hacettepe University

as a Partial Fulfillment to the Requirements

for the Award of the Degree of Master of Sciences

in Mechanical Engineering.

2020

ABSTRACT

THE DETERMINATION OF THE FUNCTIONAL FATIGUE LIFE OF HIGH TEMPERATURE SHAPE MEMORY ALLOYS AFTER COLD ROLLING PROCESS

Mustafa Sefa VELİPAŞAOĞLU

Master of Sciences, Department of Mechanical Engineering

Supervisor: Doç. Dr. Benat Koçkar

June 2020, 61 Pages

Shape memory alloys (SMA) are unique materials due to their shape recover characteristics. These materials can work against load with their shape recover ability, which lead them to be used as actuators in aerospace applications. Most applications of SMAs request a large number of cycles and the transformation temperatures which are above 100 ˚C. For Ni-rich NiTi alloys, aging heat treatment, ternary element addition and plastic deformation are the known methods to adjust the transformation temperatures and to improve the cyclic stability. Achieving the cyclic stability in terms of the transformation temperatures and the actuation strain is an important objective for the actuation applications of shape memory alloys. In this study, $Ni_{50,3}Ti_{29,7}Hf_{20}$ high temperature alloy was used due to its high transformation temperatures, high strength and promising cylic stability. The functional fatigue properties of the cold-rolled and aged $Ni_{50,3}Ti_{29,7}Hf_{20}$ high temperature shape memory alloy were investigated to exhibit the effect of cold rolling together with aging on functional fatigue behaviour. The material was produced with high-purity Ni, Ti and Hf elements via vacuum

induction melting under high purity argon atmosphere. One batch of the material was only solutionized at 1050°C for 2 hours. Another batch was solutionized and aged at 550°C for 3 hours. The other two batches are solutionized, cold rolled by 5 and 10% and aged, respectively. The solutionizing and the aging heat treatments were accomplished in a vertical cylindrical furnace under high purity argon atmosphere. The samples were rolled with a laboratory-type rolling mill at room temperature. The samples were cut to flat dog bone geometry to perform the load-biased heating-cooling experiments and the functional fatigue experiments. Stress-free transformation temperatures were measured by using Differential Scanning Calorimetry (Perkin Elmer 8000). The load-biased heating-cooling experiments were done by UTEST 50 kN servo-mechanical test instrument. These experiments were performed to determine the transformation temperatures and to observe the shape memory behaviour of the samples under different stress magnitudes. The functional fatigue experiments were conducted with a custom-built functional fatigue test setup to determine the functional fatigue life of all the samples. Load-biased heating-cooling experiments showed that the actuation strain decreases with the increase of the percentage of cold rolling due to the texture formation or the decrease in the transforming volume. The cold rolling induces high amount of dislocations to the matrix such that these dislocations increase the strength of the alloy and inhibit the martensite-austenite boundary movement. Additionally, the critical shear stress for slip increases and thus the irrecoverable strain decreases. The results of the functional fatigue experiments proved that the cold rolling improves the cyclic stability in terms of actuation strain, dimensional stability and transformation temperatures. However, the fatigue life of the alloy was diminished due to the increase in the crack formation with the increase in cold rolling percentage. NiTiHf alloys are high strength alloys such that it is very difficult to deform them. Cold rolling process may form more cracks and these cracks can easily propagate during the fatigue cycles. Therefore, the functional fatigue life decreases with the increase in cold rolling percentage.

ÖZET

YÜKSEK SICAKLIK ŞEKİL HAFIZALI ALAŞIMLARIN SOĞUK HADDELEME İŞLEMİ SONRASI FONKSİYONEL YORULMA ÖMÜRLERİNİN TAYİNİ

Mustafa Sefa VELİPAŞAOĞLU

Şekil hafızalı alaşımlar, şekil geri kazanma özelliklerinden dolayı özel malzemelerdir. Bu malzemeler şekil geri kazanma yetenekleri sayesinde yüke karşı iş yapabilmektedir. Bu özellik onların havacılık uygulamalarında eyleyici olarak kullanılmasına olanak sağlar. Uzun çevrim ömrü ve dönüşüm sıcaklıklarının 100 ˚C'nin üzerinde olması, şekil hafızalı alaşımların bir çok uygulaması için istenen özelliklerdir. Nikelce zengin NiTi alaşımlarında, dönüşüm sıcaklıklarını istenen seviyeye göre ayarlamak ve çevrimi daha stabil hale getirmek için ısıl işlem ile yaşlandırma, üçüncül element eklentisi ve plastik deformasyon en bilinen yöntemlerdir. Dönüşüm sıcaklıkları ve eyleyici gerinimi açısından çevrimsel kararlılığı sağlayabilmek, şekil hafızalı alaşımlar için eyleyici uygulamalarındaki en önemli hedeftir. Bu çalışmada yüksek dönüşüm sıcaklıkları, yüksek dayanımı ve çevrimsel kararlılık yönünden umut verici olmasından dolayı, $Ni_{50,3}Ti_{29,7}Hf_{20}$ yüksek sıcaklık şekil hafızalı alaşımı kullanılmıştır. Bu çalışmada, soğuk haddeleme ardından yaşlandırmanın fonksiyonel yorulma davranışına etkisini göstermek amacıyla, soğuk haddelenmiş ve yaşlandırılmış $Ni_{50,3}Ti_{29,7}Hf_{20}$ yüksek sıcaklık şekil hafızalı alaşımının fonksiyonel yorulma özellikleri incelenmiştir. Malzeme, yüksek saflıkta Ni, Ti ve Hf elementleri ile, yüksek saflıkta argon

atmosferinde, vakumda endüklemli eritme yöntemi kullanılarak üretilmiştir. Çalışmadaki bir grup malzemeye sadece 1050 ˚C'de 2 saat çözündürme ısıl işlemi uygulanmıştır. Bir diğer gruba çözündürme ve ardından 550 ˚C'de 3 saat yaşlandırma ısıl işlemi uygulanmıştır. Diğer iki gruba sırasıyla çözündürme, %5 ve %10 soğuk haddeleme ve yaşlandırma ısıl işlemi uygulanmıştır. Çözündürme ve yaşlandırma ısıl işlemleri, dikey silindirik fırında yüksek argon atmosferinde gerçekleştirilmiştir. Numuneler labaratuar tipi hadde kullanılarak oda sıcaklığında haddelenmiştir. Sabit yük altında ısıtma soğutma deneyleri ve fonksiyonel yorulma deneylerinde kullanılmak üzere numuneler yassı köpek kemiği şeklinde kesilmiştir. Diferansiyel taramalı kalorimetre (Perkin Elmer 8000) ile numunlerin yüksüz dönüşüm sıcaklıkları ölçülmüştür. Sabit yük altında ısıtma soğutma deneyleri, numunelerin dönüşüm sıcaklıklarını belirlemek ve farklı yükler altında şekil hafıza davranışlarını gözlemlemek için UTEST 50 kN servo mekanik deney cihazı kullanılarak gerçekleştirilmiştir. Fonksiyonel yorulma ömürlerinin tayini için özel üretim fonksiyonel yorulma test düzeneği kullanılarak fonksiyonel yorulma deneyleri tamamlanmıştır. Sabit yük altında ısıtma soğutma deneyleri sonucunda, doku oluşumundan veya dönüşen hacmin azalmasından kaynaklı olarak soğuk haddeleme yüzdesi arttıkça eyleyici geriniminin düştüğü görülmüştür. Soğuk haddeleme, matriste yüksek miktarda dislokasyona neden olmaktadır öyle ki bu dislokasyonlar alaşımın dayanımını arttırır ve martensit-östenit sınır hareketine engel teşkil eder. Ek olarak kayma için gerekli kritik kayma gerilimi artar ve böylece geri dönüşemeyen gerinim azalır. Fonksiyonel yorulma deneyleri, soğuk haddeleme prosesinin, çevrimsel kararlılığı; eyleyici gerinimi, boyutsal kararlılık ve dönüşüm sıcaklıkları açısından geliştirdiğini göstermiştir. Fakat soğuk haddeleme yüzdesi arttıkça çatlak oluşumu arttığından dolayı alaşımların yorulma ömrü azalır. NiTiHf alaşımları yüksek dayanımlı alaşımlar oldukları için deforme etmek oldukça zordur. Soğuk haddeleme prosesinin matriste daha fazla çatlak oluşturma ihtimali yüksektir ve bu çatlaklar yorulma çevrimleri sırasında kolayca ilerleyebilir. Bundan dolayı, fonksiyonel yorulma ömrü soğuk haddeleme yüzdesi arttıkça azalır.

Anahtar Kelimeler: Yüksek Sıcaklık Şekil Hafızalı Alaşımlar, Fonksiyonel Yorulma, Yaşlandırma, Soğuk Haddeleme, Dönüşüm Sıcaklıkları, Eyleyici Gerinimi

ACKNOWLEDGEMENTS

First of all, I would like to thank my supervisor Assoc. Prof. Dr. Benat Koçkar for providing guidance, excellent support and never-ending patience throughout my study.

I would like to thank to my all labmates in Hacettepe University Advanced Materials Labaratory for their support, assistance and useful critiques, especially to Halil Onat Tuğrul, Hasan Hüseyin Saygılı and Oğulcan Akgül.

I thank to my company Turkish Aerospace for their support in providing academic leave for my master's degree.

I would like to express my special thanks to my father Adnan Menderes Velipaşaoğlu, my mother Hatice Velipaşaoğlu, my brother Ali Kerem Velipaşaoağlu, my sister Aliye Merve Küçükbaycan, her husband Arda Küçükbaycan and my lovely niece Eylül Küçükbaycan for their support that they have always given to me.

Finally, I thank to my fiancee Selin Demir for always motivating and encouraging me to finish my master's degree in this very intense academic period.

Mustafa Sefa VELİPAŞAOĞLU

Haziran 2020, Ankara

TABLE OF CONTENTS

LIST OF TABLES

LIST OF FIGURES

SYMBOLS AND ABBREVIATIONS

Symbols

Ni   Nickel

Ti   Titanium

Hf   Hafnium

Abbreviations

M_s Martensite Start Temperature

M_f Martensite Finish Temperature

A_s Austenite Start Temperature

A_f Austenite Finish Temperature

TT   Transformation Temperature

SMA   Shape Memory Alloy

SME   Shape Memory Effect

FF   Functional Fatigue

HTSMA   High Temperature Shape Memory Alloy

DSC   Differential Scanning Calorimetry

ECAE   Equal Channel Angular Extrusion

UCT   Upper Cycle Temperature

S   Solutionized

S-A   Solutionized - Aged

S-CR5-A   Solutionized - 5% Cold-Rolled - Aged

S-CR10-A   Solutionized - 10% Cold-Rolled - Aged

1. INTRODUCTION

Shape memory alloys (SMA) are special alloys due to their extraordinary shape recover characteristics. After deformed, they can remember the pre-deformed shape. This unique ability occurs when the material is deformed under M_f and then heated over the A_f. The shape recovery is observed upon heating. The deformation in the martensite is accommodated via twinning instead of slip such that the shape change is reversible. These materials can work against load with their shape recover ability, which lead them to be used as actuators in aerospace applications.

Most applications of SMAs request a large number of cycles. For this reason, achieving the cyclic stability is an important goal for the SMAs. The cyclic stability can be explained as the dimensional stability such that shape change should not be seen throughout the thermomechanical cycles. Additionally, actuation strain and the transformation temperatures should stay constant throughout the cycles. The large evolution in TTs and the actuation strains from cycle to cycle make the material inconvenient for the actuation applications. The functional fatigue is the observation of the changes in these critical properties throughout cycles.

NiTi SMAs are the most preferred alloy to study due to their good cyclic stability and mechanical features [1, 2]. TTs of NiTi SMAs that are below 100˚C limit the application of these alloys, especially in aerospace industry. Therefore, the SMAs with high TTs are used to expand the usage of the SMAs. The SMAs with TTs above 100˚C are defined as "High Temperature Shape Memory Alloys (HTSMAs)".

The TTs of NiTi SMAs can be raised above 100˚C with element addition to this binary systems. The proper additional ternary elements which can be found in literature are Hf, Zr, Pd, Au, Pt to NiTi alloys [3, 4, 5, 6]. Among these elements, Pd, Au and Pt are relatively expensive. So, they are not suitable for most of the commercial applications. This is the reason that the researches are mostly concentrated on Hf and Zr as a ternary element. The oxygen affinity of Zr makes the alloys brittle [7, 8]. Because of this disadvantage of Zr, Hf is the most preferred and promising ternary element for NiTi alloys [5, 9, 10, 11, 12, 13].

The nano-scale precipitations can be generated by means of conducting aging heat treatment in Ni-rich NiTiHf HTSMAs. The precipitates change the mechanical and chemical features of alloys. They provide a raise in critical shear stress to slip [10]. The increase in critical shear stress to slip is important to obtain better cyclic stability. Because, it can minimize the plastic accomodation with strain hardening via introducing dislocations [10]. The formation of precipitation causes the decrease of the Ni content such that the TTs increase owing to decrease of Ni in matrix [14, 15, 16]. Also, the precipitation size effect on shape memory behavior and microstructure of the NiTiHf alloys has been reported in many studies [5, 14, 17].

$Ni_{50,3}Ti_{29,7}Hf_{20}$ HTSMAs is among most promising HTSMAs, because their cyclic stability can be enhanced with nanoprecipitate formation. Moreover, the transformation temperatures of this composition can be increased with precipitation heat treatments. In the literature, there are studies which observe the effect of the nano precipitates on cyclic stability and shape memory behavior for $Ni_{50,3}Ti_{29,7}Hf_{20}$ HTSMAs [18, 19, 20, 21]. Also, there are studies which focused of the aging effect of different temperatures and different durations like the study of Karaca and his colleagues. The mentioned study shows that the aging at 550˚C for 3 hours gives the optimum results for $Ni_{50,3}Ti_{29,7}Hf_{20}$ HTSMA in terms of TTs and cyclic stability [22]. Besides all these, Karaman's group worked on cyclic stability of NiTiHf alloy with functional fatigue tests [23, 24]. Kockar's group showed that the nano-precipitates which are formed via aging at 550˚C for 3 hours improve the cyclic stability of $Ni_{50,3}Ti_{29,7}Hf_{20}$ HTSMA [21].

The cyclic stability of NiTi based SMAs can be enhanced via deformations such as extrusion, cold and warm rolling. This occurs because of the reduction in grain size and the growth in dislocation density. Because, the critical shear stress to slip accommodation is raised with reduction of the grain size via preventing dislocation motion [10, 25, 26, 27, 28]. In addition, Kockar's group exhibited the comparison of the transformation behavior and shape memory features like the irrecoverable strain, actuation strain, thermal hysteresis and transformation temperatures under increasing constant stress with two different thermomechanical processing condition which are Cold Rolling and Cold Rolling with aging by using $Ni_{50,3}Ti_{29,7}Hf_{20}$ HTSMA. The cold rolled sample in mentioned study has 10 percent thickness reduction [29].

2

This study presents the effect of cold rolling and aging after cold rolling on the functional fatigue behaviour of $Ni_{50,3}Ti_{29,7}Hf_{20}$ HTSMA. Additionaly, this study includes the effect of 5 percent cold rolling in addition to 10 percent cold rolling to transformation behaviors and cyclic stability of aforementioned Ni-rich NiTiHf alloy. It should be stated that, this is the first study which focused on the cold rolling effect together with aging effect on functional fatigue properties of $Ni_{50,3}Ti_{29,7}Hf_{20}$ HTSMA. With this purpose, the TTs and cyclic stability of aged and aged after cold rolling samples are compared.

It is noted that the all samples are firstly solutionized before aging and cold rolling operations to homogenize the chemistry of the alloy. For simplicity, the samples which were thermally and thermomechanically treated are coded to keep the text of the thesis as simple as possible. "S" will be used for solutionized, "A" will be used for aged samples and "CR" will be used with the number of percentage for cold-rolled samples throughout the text. The samples in this study are S, S-A, S-CR5-A and S-CR10-A. The order of the abbreviations refers the order of the applied procedures.

2. THEORY AND LITERATURE

Shape memory alloys (SMA) are named with this name due to the capability to return to a predetermined shape when heated. After an obvious deformation, they can recover their shapes with thermoelastic martensitic transformation upon heating to pre-determined temperatures. They are good candidates as actuators under favour of their strength, fatigue characteristic and high power to weight ratios [1].

The shape change upon phase transformation occurs with two types of accommodation. One of them is slip. In the slip mechanism, the boundaries are broken and the shape is permanent. But the twinning is reversible. Twinning is the key mechanism in the shape memory effect. SMAs are transformed to martensitic structure via twinning. After stress is applied to while the alloy is in martensite, twins are reoriented to create de-twinning structure. The twin boundaries have low energy. Also, the boundaries have good mobility such that the shape change due to applied stress can be accommodated relatively easier [30].
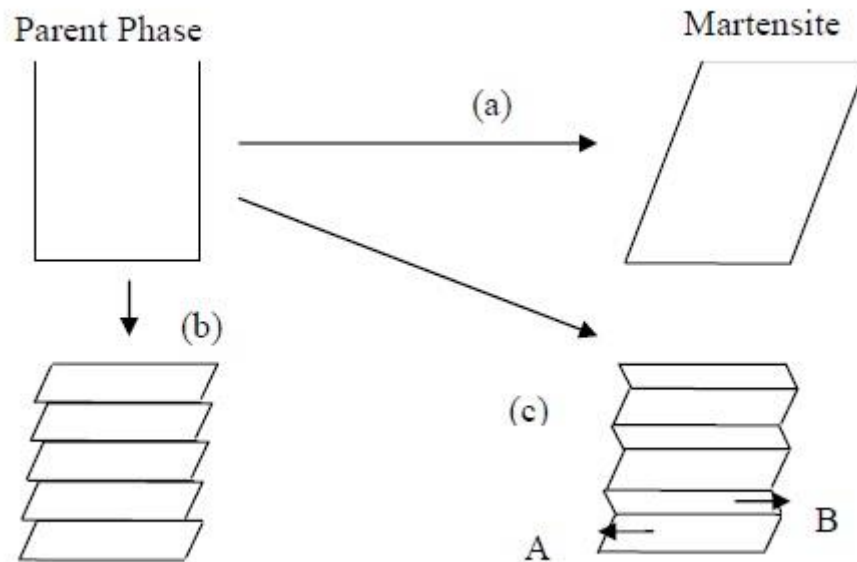
Figure 2.1-1. "a) Shape change upon phase transformation b) represents the accommodation of external strain by slip, c) represents the accommodation of external strain by twin" [31].

The shape memory effect (SME) is because of thermoelastic phase transformation and twinning is the mechanism to accommodate shape change and to provide reversibility of the shape change. If SMA is deformed in martensitic phase, it can return to predeformed shape when heated to austenitic phase [30]. As a clarification, there is a triaxial graph as illustrated in Figure 2.1-2. The SMA is in austenitic phase at the first point without any load. From first point to second point, temperature decreases and the structure is transformed to self-accomodated martensite by twinning. From second point to third point, the stress is applied and the detwinning process occurs. From third point to fourth point, applied stress is removed and the elastic strain is recovered. In fourth point, the structure is plastically deformed in detwinned martensite without load. From fourth point to first point, the structure is heated to austenitic phase and the recovery takes place. This phenomena is named as shape memory effect [32].
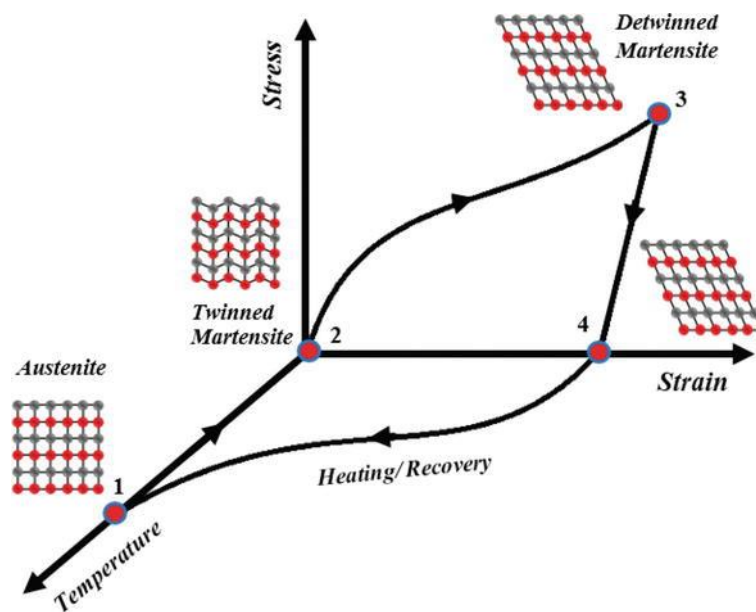
Figure 2.1-2.   The illustration graph of SME [32].

There are some important parameters of SMAs to evaluate the usability for the applications. They are TTs, irrecoverable strain, actuation strain, transformation strain and hysteresis. Figure 2.1-3 shows the representative strain-temperature behavior of SMAs. The graph in Figure 2.1-3 starts after the constant stress is applied to the alloy in austenitic phase. In this case, the austenitic structure is elastically deformed. When the temperature is decreased sufficiently, the phase transformation occurs from austenite to martensite. The blue line represents the cooling. M_s is the martensite start temperature and M_f is the martensite finish temperature. Below M_f temperature, the structure is completely transformed into martensite. Afterwards, when the temperature is increased, the phase transformation occurs from martensite to austenite. During this transformation, the shape recovery happens. The red line represents the heating. A_s is the austenite start temperature and A_f is the austenite finish temperature. Above A_f temperature, structure is fully transformed into austenite, shape is recovered [30].
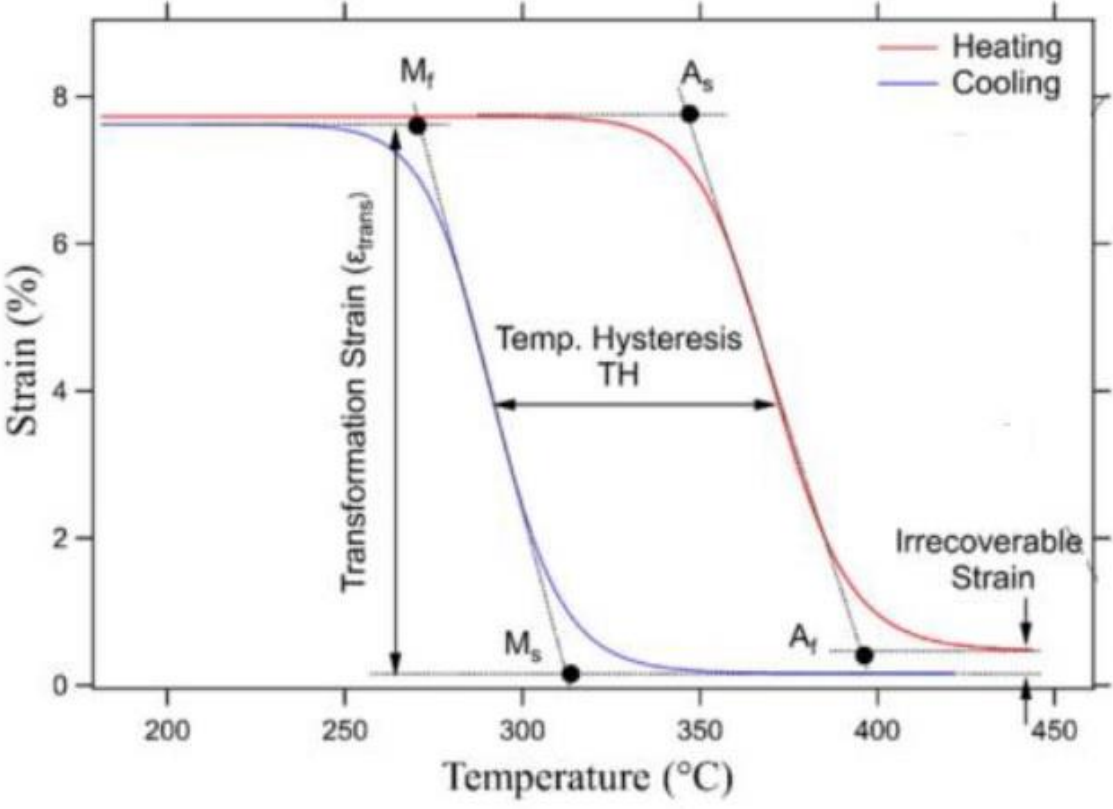
Figure 2.1-3.   A typical strain vs. temperature behaviour of SMAs [33].

The total strain change throughout phase transformation is defined as the transformation strain. Sometimes, SMAs are plastically deformed during transformation and they cannot recover all deformation. When this happens, the recoverable strain is not equal total transformation strain due to the appearance of irrecoverable strain as indicated in Figure 2.1-3. It can be seen that the heating and cooling lines are not coincided. There is a difference between heating and cooling lines as indicates in Figure 2.1-3. This difference is named as hysteresis. The hysteresis can be explained with the frictional energy during transformation because of the martensite-austenite transformation and the dissipation of elastic stored energy [30].

While working with these strain-temperature diagrams for SMAs, the exact temperature points for the beginning and the end of the transformations may not be obtained exactly. Therefore, to determine the TTs, tangent lines are used as shown in Figure 2.1-3. The intersections of the tangent lines provide the TTs. Hysteresis is determined from curves by taking the temperature difference from the middle points of the curves.

SMAs can be evaluated with the help of these parameters. For the most high temperature actuation applications, the transformation temperatures must be above 100˚C to prevent unintended actuations at ambient temperatures. Also, resistance to higher loads and higher magnitudes of actuation strain are generally desired to provide higher work output. The other most desired feature for SMAs is long fatigue life with less irrecoverable strain.

2.1. Conventional Shape Memory Alloys

Most utilized and studied SMAs are Cu, Fe and NiTi-based alloys due to their mechanical and functional shape memory properties.

2.1.1. Cu-based Shape Memory Alloys

Cu-Al and Cu-Zn based SMAs are most known and studied Cu-based SMAs. Cu-based SMAs would be preferred due to their low cost. While the TTs of Cu-Zn SMAs are under -50˚C, the TTs of Cu-Al SMAs are over 100˚C [34, 35]. The method of adding ternary alloying element is used to approach the desired transformation temperatures, to enhance the shape memory characteristics and to develop the alloy mechanically. Most promising Cu-based alloys with ternary addition are Cu-Zn-Al, Cu-Al-Mn and Cu-Al-Ni [35].

In comparison with each other Cu-based SMAs, while Cu-Al-Ni has enhanced mechanical features, Cu-Zn-Al has high and relatively good TTs. The distinctive feature of Cu-Al-Mn over the other Cu-based SMAs is its high ductility [35].

The most significant handicap of Cu-based SMAs in terms of mechanical features, their low resistance to grain boundary fracture. The fracture can occur easily in these alloys [36]. Regarding to this feature, Cu-Al-Mn and Cu-Zn-Al SMAs are relatively better than another Cu-based alloys due to their relatively higher ductility [35]. The TTs of Cu-Zn-Al above 100˚C. But the shape memory features of the Cu-Zn-Al not as good as NiTi based SMAs. They are not stable enough for the actuation applications [37, 38].

2.1.2. Fe-based Shape Memory Alloys

The shape memory properties of Fe-based are weaker than Cu-based and NiTi-based SMAs. But they are cheaper than another SMAs. Some of Fe-based SMAs like Fe-Ni-Co-Ti, Fe-Pt Fe-Pd have low hysteresis values. Their hysteresis are below 10˚C. Other Fe-based SMAs like Fe-Ni-C, Fe-Mn-Si, show thermal hysteresis of around 150˚C [39].

Fe-Mn-Si alloys are promising with Ni, Co and Cr additions among the others. These additions enhance the mechanical features. These alloys have huge hysteresis values. For this reason, they are not capable for superelasticity and two way SME. Consequently, they are not good candidates for most engineering applications as a SMA [39].

2.1.3. NiTi-based Shape Memory Alloys

In contrast with Fe-based and Cu-based SMAs, NiTi-based SMAs have high ductility, outstanding corrosion resistance and superior shape recover abilities [40]. Under the favor of these unique features, NiTi-based SMAs are most studied SMAs.

There are many researches which concentrated on the influence of thermomechanical treatments on shape memory features of NiTi alloys since the TTs of NiTi-based SMAs are under 100˚C. This is a disadvantage for most high temperature applications. The studies show that thermomechanical treatments and Ni content in the matrix are very effective on the TTs and shape memory characteristics. [6, 20, 22].

The TTs of Ni-rich SMAs can be increased with the depletion of Ni in the matrix [14]. This decrease can be achieved with aging heat treatment. With aging heat treatment, Ti_3Ni_4 precipitations are formed in matrix and these precipitations cause the depletion of Ni content [41]. It provides to an increment in TTs. Also, Ti_3Ni_4 precipitates help to maintain cyclic and dimensional stability because they enhance critical shear stress to slip. The formation of these precipitates inhibits dislocation formation during transformation and hence the stability can be enhanced [41, 42, 43]. Miyazaki's study showed that the M_s temperatures of near equiatomic NiTi SMAs are not influenced from heat treatments since the aging do not form precipitates in matrix [44].

2.2. High Temperature Shape Memory Alloys (HTSMAs)

The aging heat treatment of NiTi-based SMAs increases transformation temperatures as mentioned in previous section. But the transformation temperatures cannot reach to the desired values for high temperature application. For most actuation applications in aerospace industries, the transformation temperatures must be above 100°C.

The other known method is adding ternary alloying element to enhance the TTs. The common options to NiTi binary alloys to enhance TTs are Zr, Pd, Hf, Au and Pt. So, there are a lot of study in literature about these alloys as a ternary addition to NiTi SMAs [3, 4, 12, 45]. Pd, Au and Pt are comparatively costly than that of the other options. Therefore, they are not good choices for commercial applications. Hence, there are more studies which focused on Hf and Zr ternary elements. Zr is less favored than Hf, since the high oxygen affinity of Zr causes brittleness [7, 8]. Because of this significant disadvantage, the application of Zr is limited. Also, Hf addition provides higher work output than Pd and Pt additions as well as the efficiency in improving the TTs [22]. As a summary, Hf is the most promising ternary element addition to NiTi-based SMAs [10, 12, 14, 17, 19, 22, 23, 33, 46].

2.3. NiTiHf High Temperature Shape Memory Alloys (HTSMAs)

It is known that Hf insertion to NiTi SMAs with spending of Ti increase the transformation temperatures according to Potapov's study [47]. In this study, Ni lean $Ni_{49.8}Ti_{50.2-x}Hf_x$ alloy with x varying from 8 to 25 was used. The study shows that the transformation temperatures and Af-As, Ms-Mf transformation intervals increment with Hf amount [47]. Another study

indicates that Ni lean NiTiHf alloys exhibit a brittle nature with Ti content increase at the expense of Ni with a constant Hf content of 10%. In this study, $Ni_{50}Ti_{40}Hf_{10}$, $Ni_{49}Ti_{41}Hf_{10}$ and $Ni_{40}Ti_{50}Hf_{10}$ alloys were used [48]. These studies show that Ni-rich NiTiHf high temperature SMAs are more promising in terms of shape memory and mechanical features. The further studies are more focused on mentioned alloys.

The effect of aging on transformations and microstructure in NiTiHf SMA has been demonstrated in X.L. Meng's study [16]. The aging heat treatment was applied on $Ni_{50.6}Ti_{29.4}Hf_{20}$ SMA at 550˚C and $(Ti+Hf)_3Ni_4$ precipitates were formed. The study shows that the aging heat treatment improves the TTs detectably and $(Ti+Hf)_3Ni_4$ precipitates strengthen the matrix. It provides an improvement in the TTs and thermal stability [16].

The study of Karaca and his coworkers exhibits the effects of nanoprecipitations on $Ni_{50.3}Ti_{29.7}Hf_{20}$ alloy [22]. This alloy is the same one which has been used in this study. The aging heat treatment was applied to $Ni_{50.3}Ti_{29.7}Hf_{20}$ alloy at different temperatures in between 300˚C and 900˚C. The higher TTs are achieved via aging for 3 hours at 650˚C. However, the heat treated sample shows comparatively weak shape memory features because of large precipitation size. On the other hand, the aging for 3 hours at 550˚C gave the optimum results for better shape memory properties [22]. This study also proved that the nanoprecipitates increase the transformation temperatures and improve thermal stability due to precipitation hardening [22].
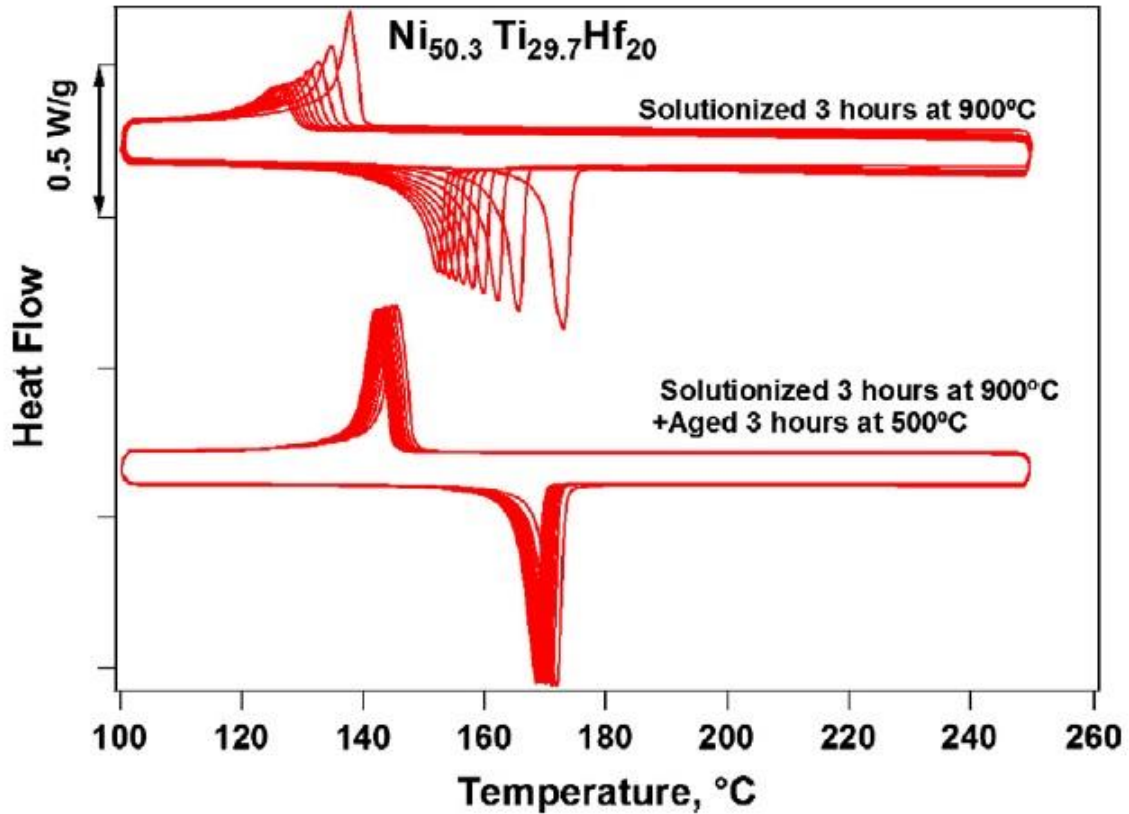
Figure 2.3-1. Effect of aging on the cyclic stability of $Ni_{50.3}Ti_{29.7}Hf_{20}$ [22].

2.4. Functional Fatigue of NiTi Shape Memory Alloys

Kockar's team showed that the effect of aging heat treatment on the functional fatigue (FF) properties of $Ni_{50.3}Ti_{29.7}Hf_{20}$ HTSMAs [21]. In their study, the FF behavior and the performance of the extruded and aged samples were investigated. They proved that the aging at 550°C for 3 hours improves fatigue life of the alloy. Also, the cyclic stability has been enhanced with aging in terms transformation temperatures and actuation strain [21].

Karaman and his co-workers worked on FF life of $Ni_{50.3}Ti_{29.7}Hf_{20}$ HTSMAs as well. In one of his studies, he focused on upper cycle temperature (UCT) effect on FF properties of the mentioned alloy [23]. The samples were aged at 550°C for 3 hours. The experiments were performed under each applied stress and the samples were heated to different UCTs. It was shown that with the increment of the applied stress and UCT, fracture occurs earlier, in other words, the samples show shorter fatigue life. As the UCT increases, the actuation strain

increases. The crack propagation accelerates due to the expansion and contraction of cracks [23].

In another study of Karaman and his team, the effect of the amount of applied stress on FF properties of $Ni_{50.3}Ti_{29.7}Hf_{20}$ HTSMA was investigated [24]. It is proved that the amount of applied stress has a noticeable effect on actuation behavior of aged HTSMAs. Increment in applied stress cause a growth in actuation strain and this growth causes a decrease in fatigue life [24].

In addition to these studies, the same group investigated the impact of microstructure on FF behavior of $Ni_{50.3}Ti_{29.7}Hf_{20}$ HTSMA [49]. In this study, they formed precipitates with different sizes with different heat treatments. It was demonstrated in this study that the larger precipitates in matrix provide better fatigue life with spending of actuation strain. Additionally, they lead to observe significant irrecoverable strain [49].

2.5. The Effect of Severe Deformations on NiTi SMAs

As stated in the previous sections, to enhance critical stress to slip is a promising way to provide better cyclic stability due to minimizing the plastic accommodation via introducing dislocations [10]. Conventional and the Severe Plastic Deformation (SPD) methods like extrusion, drawing, cold-rolling and Equal Channel Angular Extrusion (ECAE) can induce very large strains and dislocations. If the deformation is applied at ambient temperatures the dislocation formation becomes more prominent. However, the cold deformation reduces the transformation temperatures extremely without additional heat treatment. This is reported by the previous studies for severely deformed NiTi based SMAs [26, 28, 50, 51].

Kockar et.al proved that the dimensional stability of NiTiHf SMAs can be enhanced with SPD via ECAE and cold drawing plus annealing at low temperature [10]. There are other studies which showed that the plastic deformations enhance the cyclic stability of these alloys because of the reduction in grain size and growth in the dislocation density [26, 27, 28].

Karaman worked on $Ni_{50}Ti_{30}Hf_{20}$ near-equiatomic HTSMA and presented the study about the influence of the cold rolling with following annealing and the warm rolling. It was

presented that the cold rolling with following annealing and warm rolling improve the cyclic dimensional stability and make a better option for high temperature actuators. It should be noted that the cold rolling with subsequent annealing is more promising method than that of warm rolling in these HTSMAs [25].

Kockar's group demonstrated that the transformation temperatures of $Ni_{50.3}Ti_{29.7}Hf_{20}$ alloy can be stabilized by cold rolling with following aging. Also, they showed that the hot extrusion process with following aging as well enhance the stability of TTs. It was shown that the cold rolling and following aging processes can be an alternative thermomechanical treatment to enhance the cyclic stability since the cold rolled samples show very low irrecoverable strain magnitudes under different stress magnitudes [29].

3.   EXPERIMENTAL PROCEDURE

3.1. As-received Material

$Ni_{50,3}Ti_{29,7}Hf_{20}$ (at%) SMAs used were produced with high-purity Ti, Hf and Ni via vacuum induction melting (VIM) under high purity argon atmosphere. It is important to note that the percentages of the elements have been given in at% throughout the text of this thesis.

3.2. Solutionizing and Aging Heat Treatments

To reduce the probability of oxidation during heat treatments, tantalum foil were used to cover samples. The solutionizing and the aging were accomplished in a cylindrical furnace under high purity argon atmosphere. The samples were quenched by using water. In this study, the solutionizing were done at 1050˚C temperature for 2 hours to make more homogeneous the chemistry and microstructure of the samples. Solutionizing temperature and the time duration were chosen as 1050˚C and 2 hours respectively since NiTiHf is a very oxidative material. Therefore, high temperature and short term solutionizing was preferred to mitigate the possible oxidation problem. The aging were done with 550˚C temperature for 3 hours on $Ni_{50,3}Ti_{29,7}Hf_{20}$ alloy. This aging parameters have been already announced in the literature as the optimized conditions to achieve the highest shape memory properties and strength values [19, 22]. The samples which were solutionized and aged after solutionizing will be called as S and S-A throughout the text from this points.

3.3. Cold Rolling

The samples were rolled with a laboratory-type rolling mill for 5% and 10% in thickness reduction at room temperature. Since the cold rolled samples did not show any transformation via DSC experiment, aging heat treatment was applied on cold rolled samples to increase the transformation temperatures to relatively higher temperatures. The causes behind these observations will be shown and clarified in the later sections. The samples which were cold rolled after solutionizing and aged after cold rolling operation will be called as S-CR5-A and S-CR10-A throughout the text from this point.

3.4. Sample Preparation

DSC samples were cut to measure the TTs of the samples before and after the thermal and mechanical processes with saw precision cutter. The cutting was performed at very low speed rates and under no load condition to prevent the possible stress inducing to the samples since induced stress alters the transformation temperatures of shape memory alloys [52].

For load-biased heating-cooling and fatigue test, the samples were cut to flat dog bone geometry as shown in Figure 3.4-1 via wire electrical discharge machine (WEDM). The reason for selecting wire EDM for cutting operation was to minimize the residual stresses.
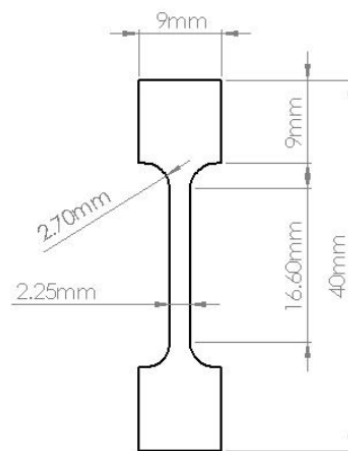
Figure 3.4-1.   The sample dimensions for load-biased heating-cooling and fatigue tests.

3.5. Differential Scanning Calorimetry (DSC)

Stress-free TTs of $Ni_{50,3}Ti_{29,7}Hf_{20}$ samples were determined by DSC (Perkin Elmer 8000). DSC tests were completed for solutionized (S) and solutionized plus cold rolled 10% plus aged (S-CR10-A) samples and the results were published in our article [29]. DSC experiments were performed on the other two samples as well which were solutionized plus aged (S-A), solutionized plus cold rolled 5% plus aged (S-CR5-A) in this study. The samples were cycled between $0^{\circ}C$ and $300^{\circ}C$ with the constant $10^{\circ}C$/min heating and cooling rates. Three cycles were performed to observe the progress in TTs throughout the cycles.

3.6. Load Biased Heating and Cooling

Load-biased heating-cooling test were done for S-A and S-CR5-A samples in addition to S and S-CR10-A samples. UTEST 50 kN test instrument was used to fulfill load biased experiments. In these experiments, tensile specimens which are illustrated in Figure 3.4-1, were placed between the grips. To prevent environmental thermal effect, insulating materials were used. The cooling and heating were performed for all samples under constant applied stress. During all experiments, the heating was performed by conduction via grips with rate of 10 °C/min. The cooling was achieved via conduction through cold water inside the copper tube surrounded the grips. An Epsilon high temperature extensometer which was located to the gage of samples were used to determine the axial strains. The test equipment is shown in Figure 3.6-1. In load-biased tests, the samples were initially heated above A_f temperature to stabilize the austenite phase in the microstructure of the samples. After the samples were loaded to 100 MPa stress in austenite, they were cooled below M_f temperature. The cooling below M_f temperature and heating above A_f temperature under constant stress level represents one cycle. After each cycle, the tensile stress was increased 100 MPa in the austenitic phase. The cycles proceeded till fracture of the samples. The strain-temperature data were generated to determine the TTs and the actuation/irrecoverable strain values under each stress magnitudes. The actuation and irrecoverable strain magnitudes were obtained from each cycles.

Figure 3.6-1. Load-biased heating-cooling test equipment.

3.7. Functional Fatigue Experiments

Functional fatigue tests were conducted with a custom-built test equipment. The cross-sectional area of samples were calculated to determine the magnitude of the constant load corresponding to 200 MPa stress. This magnitude is set as threshold level. Because the irrecoverable strain were not observed in 200 MPa stress during load-biased heating-cooling tests. All fatigue tests were performed under 200MPa constant stress level. The loading was conducted using weights while the samples were kept in austenite phase. The samples were cooled under M_f temperature and heated over A_f temperature under constant stress level. It represents one cycle. The heating/cooling rate was chosen as 15 °C/sec in this study. The samples were painted with a black paint to specify the emissivity value. The emissivity value was required to measure the temperature of the samples from gauge section by Optris CTlaser LTF-CF1 infrared thermometer. The samples were heated via the electric current passing through the samples via DC power supply. The cooling of the samples were accomplished using air nozzles with compressed air. The amount of air flow was controlled with a regulator. The displacement was determined by using a linear potentiometric displacement sensor (LPDS). To maintain the specified heating/cooling rate, integrated PI controller was used. This controller was utilized to control the electrical current and the

amount of the air flow. During these experiments, temperature and displacement data together with the number of cycles were collected and saved.
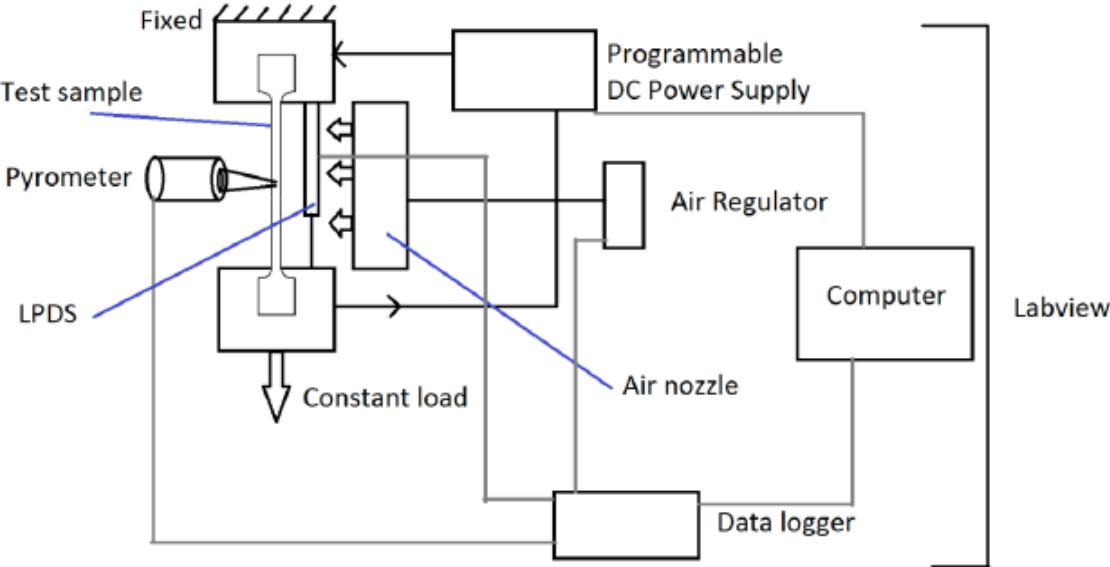

Figure 3.7-1.   The diagram of fatigue test equipment [53].

4. EXPERIMENTAL RESULTS

4.1. Differential Scanning Calorimetry (DSC)

DSC results of S, S-A, S-CR5-A and S-CR10-A samples are shown in Figure 4.1-1 and Figure 4.1-2. With these experiments, heat flow-temperature curves are generated for all samples. Figure 4.1-1 and Figure 4.1-2 show the behavior of heat flow during heating and cooling, respectively. DSC results have shown that while the aging increased the TTs, cold deformations decreased the TTs. The transformation peaks were not observed without aging in cold rolled samples depending on the huge decrease of TTs. After aging, the peaks of cold rolled samples were observed due to increment in TTs. This increment can be clarified with growth in precipitate volume. The amount of Ni in matrix decreases with formation of precipitations and it ends up with the increase of TTs. The decrease in TTs with cold rolling can be clarified with the increment of dislocation density. In addition to this, M_f temperatures of S-CR5-A and S-CR10-A cold rolled samples were not detected because the peak was not clear to determine M_f temperatures as shown in Figure 4.1-2 In the cold rolling samples, martensite stabilization occurs due to high amount of dislocation.
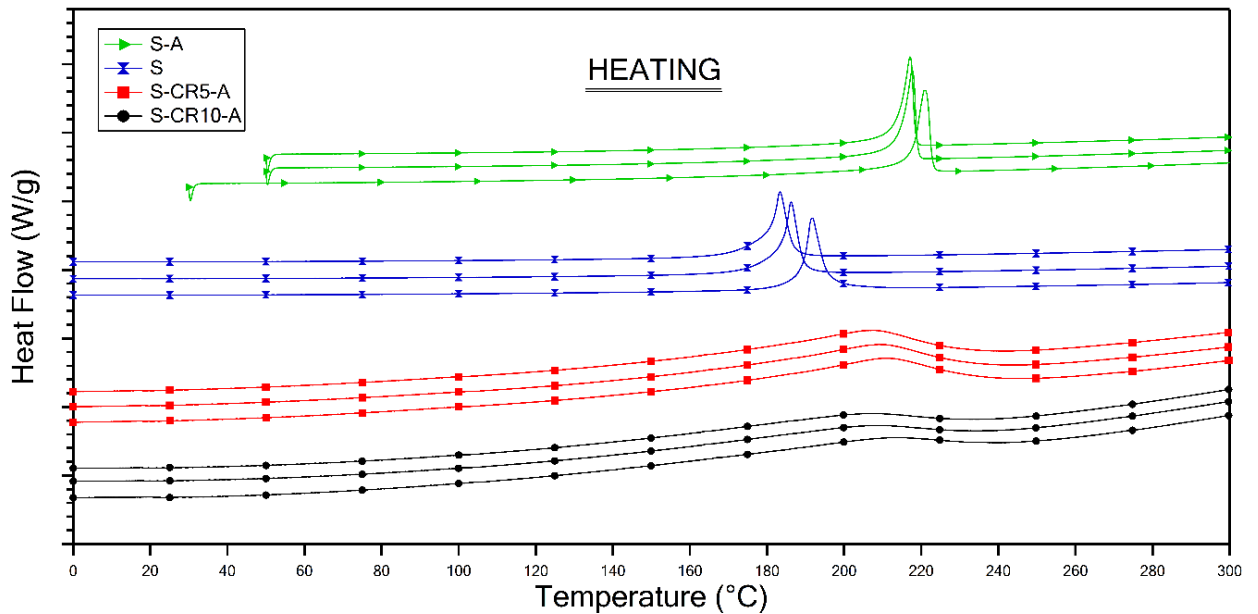

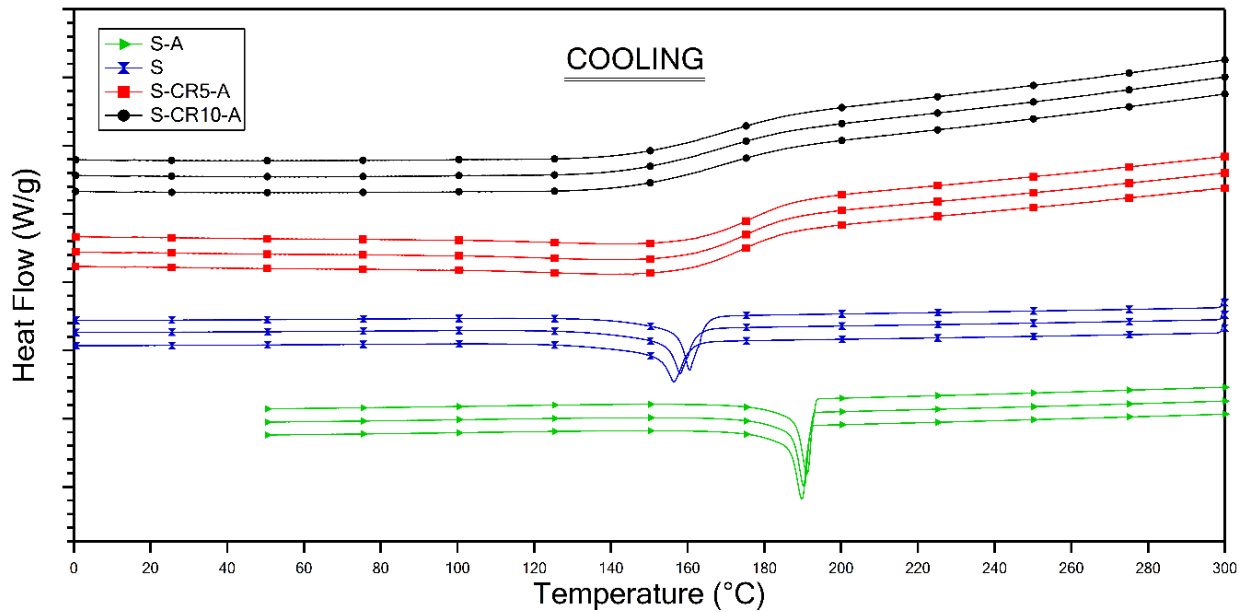Figure 4.1-1.   Heating curves of all samples obtained from DSC.

Figure 4.1-2.   Cooling curves of all samples obtained from DSC.

The TTs of samples were obtained from DSC data and are listed in Table 4.1-1. A_s and A_f were obtained from the heating curves in Figure 4.1-1, M_s and M_f were obtained from the cooling curves in Figure 4.1-2.

The following comments can be drawn from Table 4.1-1:

-   All transformation temperatures increase with aging. This is the Ni precipitate effect that mentioned above.

-   A_s temperatures decrease gradually with the increment of cold rolling rate because of the dislocation density.

-   When M_s temperatures and A_s temperatures are compared, it is obvious that the cold rolling is less effective on M_s temperatures. In 5% and 10% cold rolled samples, M_s temperatures are similar despite the deformation rate is doubled. The growth in the deformation rate from 5% to 10% is not effective on M_s temperatures. M_s temperatures of the cold-rolled samples are lower than S-A sample but higher than S sample. It can be deduced that the effect of aging to increase M_s temperatures prevails over the effect of cold rolling to decrease M_s temperatures.

-   While the A_s temperatures decrease with cold rolling even after aging, A_f temperatures are not affected much with the amount of the cold rolling percentage. So, the difference between A_s and A_f temperatures become higher.

20

- The difference of temperatures after three cycles indicate that the TTs become more stable after cold rolling.

Table 4.1-1.   TTs of all samples from DSC experiments.

Sample	Cycle	Transformation Temperatures (°C)			
		M_f	M_s	A_s	A_f
S	1	155.9	165.3	188.4	196.6
	2	153.3	163.1	180.8	190.6
	3	152.4	161.7	178.4	186.9
	Difference (°C) (3-1)	-3.5	-3.6	-10	-9.7
S-A	1	187.7	193.3	217.1	223.3
	2	187.1	192.6	212.8	219.6
	3	185.9	191.9	212.8	218.7
	Difference (°C) (3-1)	-1.8	-1.4	-4.3	-4.6
S-CR5-A	1	—	185.9	101.3	241.7
	2	—	186.9	103.9	238.4
	3	—	184.9	99	237.1
	Difference (°C) (3-1)	—	-1	-2.3	-4.6
S-CR10-A	1	—	187.5	85.1	244.5
	2	—	186.4	86	242.7
	3	—	185	85.1	241.9
	Difference (°C) (3-1)	—	-2.5	0	-2.6

4.2. Load Biased Heating and Cooling

The strain vs. temperature curves were drawn using the data from load biased heating-cooling tests and were presented in Figure 4.2-1 to 4.2-8. The figures indicate the strain vs. temperature curves for S, S-A, S-CR5-A and S-CR10-A samples under each constant stress values starting from 50 MPa to 700 MPa, respectively.
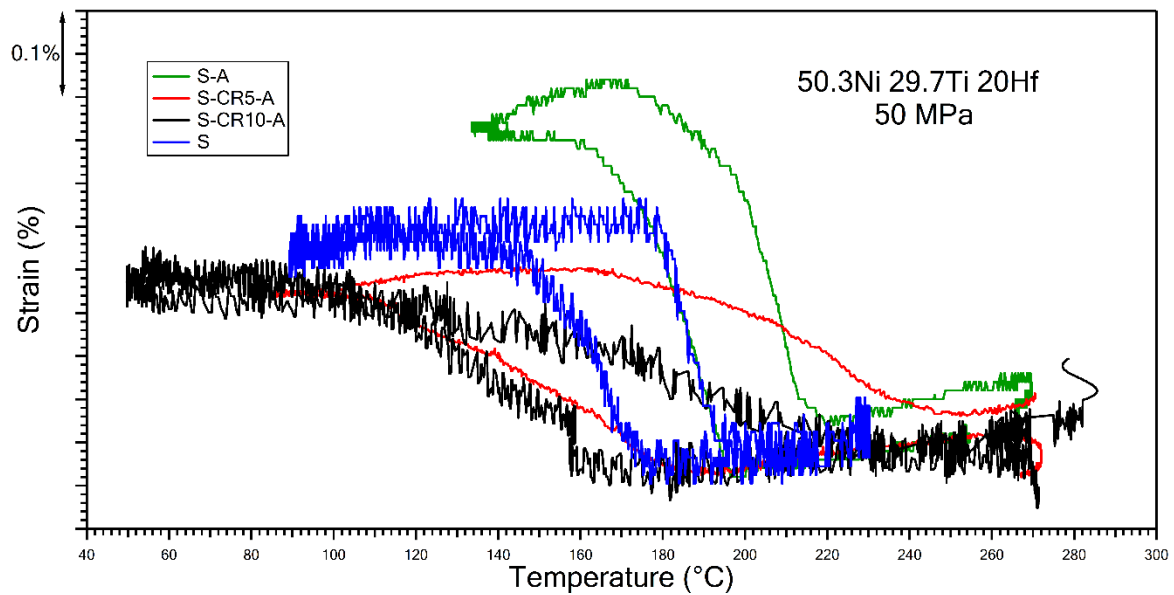
Figure 4.2-1.   Under 50 MPa applied stress, strain-temperature behaviour.
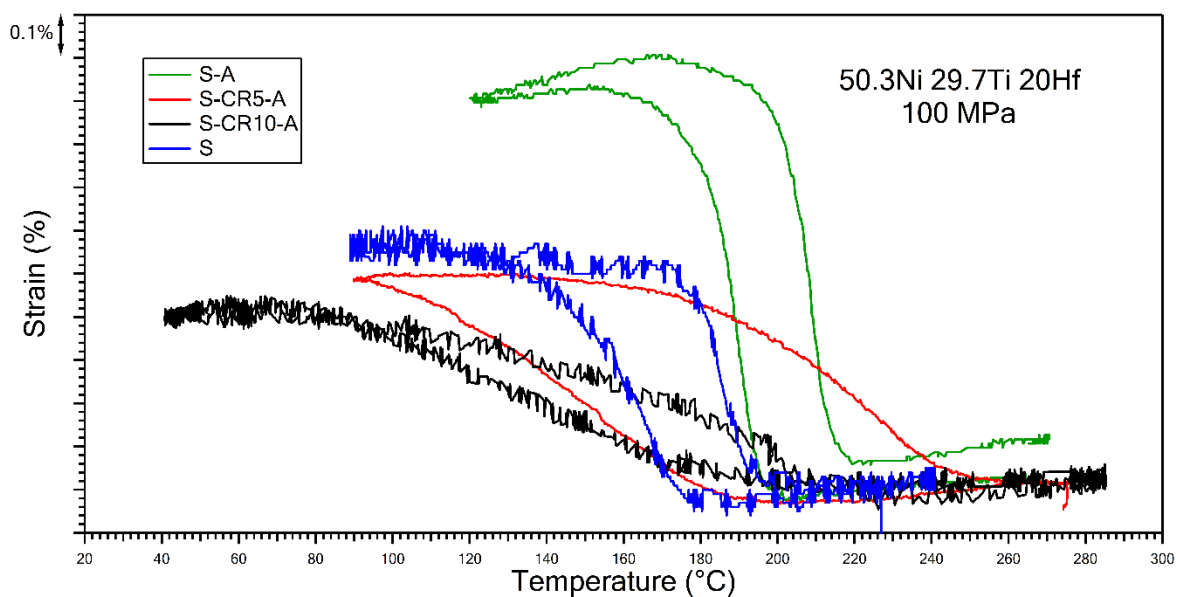
Figure 4.2-2.   Under 100 MPa applied stress, strain-temperature behaviour.
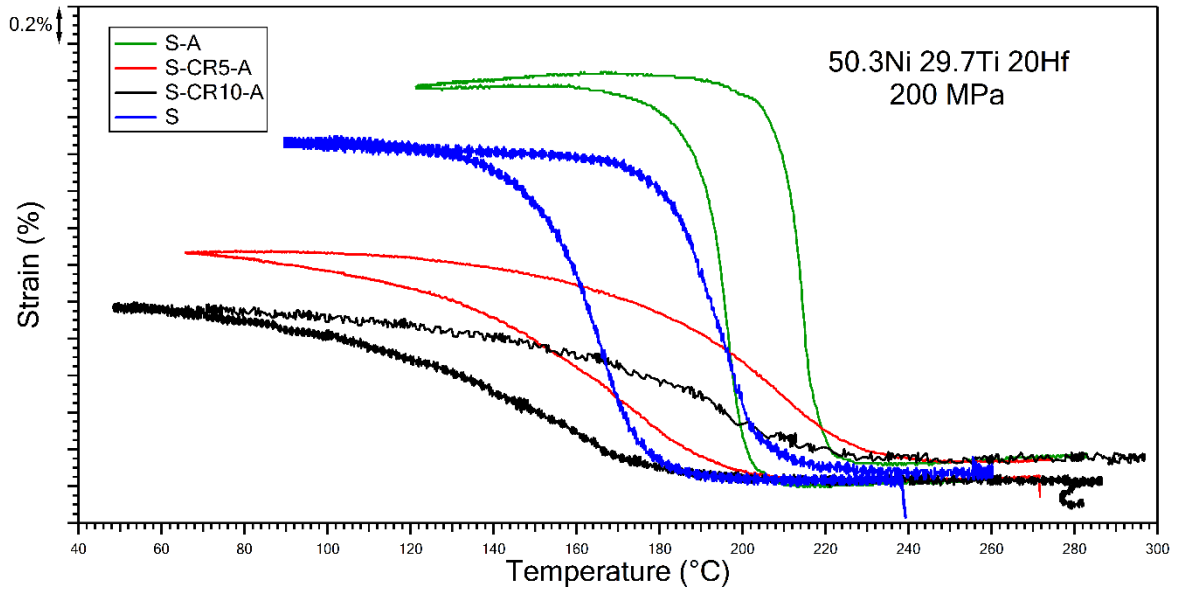
Figure 4.2-3. Under 200 MPa applied stress, strain-temperature behaviour.
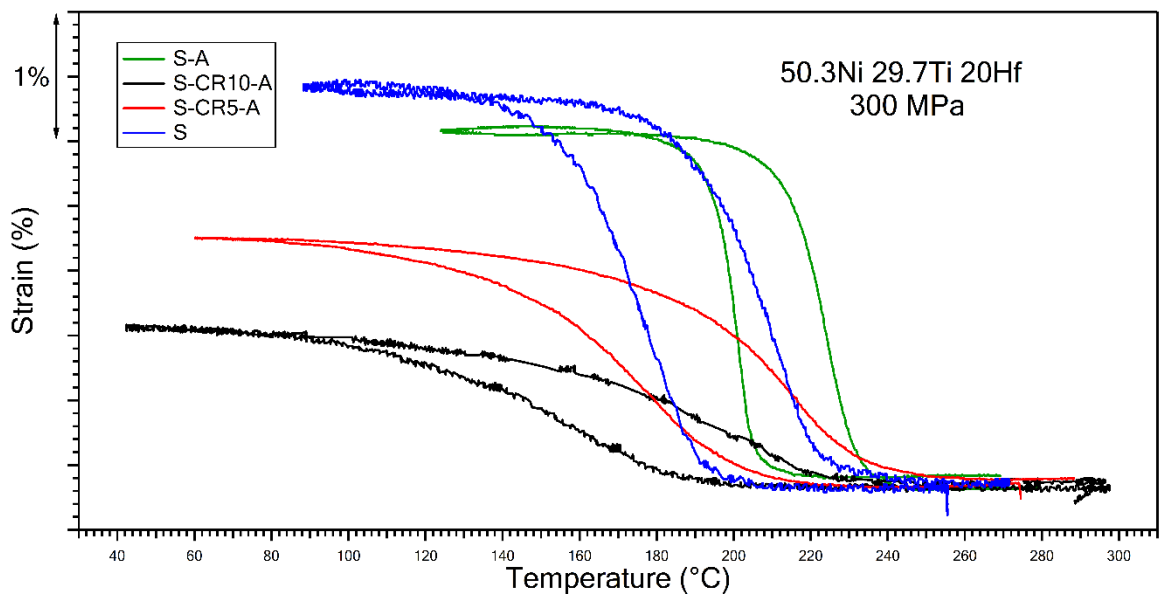
Figure 4.2-4. Under 300 MPa applied stress, strain-temperature behaviour..

Figure 4.2-5 shows that "S" samples was failed during the heating period under 400 MPa.

Figure 4.2-5. Under 400 MPa applied stress, strain-temperature behaviour.

S-CR5-A sample fractured under 500 MPa during cooling period as shown in Figure 4.2-6.

Figure 4.2-6. 500 MPa applied stress, strain-temperature behaviour.

Figure 4.2-7 shows that the fracture occurs for S-A sample at the beginning of the cooling period under 600 MPa.
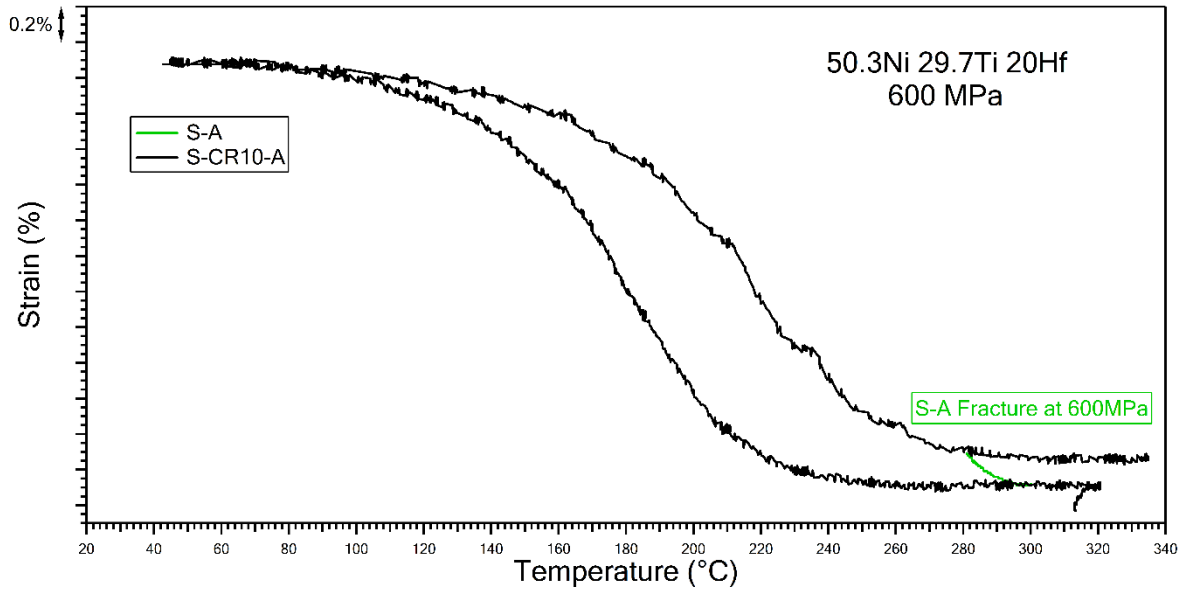
Figure 4.2-7. Under 600 MPa applied stress, strain-temperature behaviour.

S-CR10-A sample fractured under 700 MPA during cooling as shown in Figure 4.2-8.
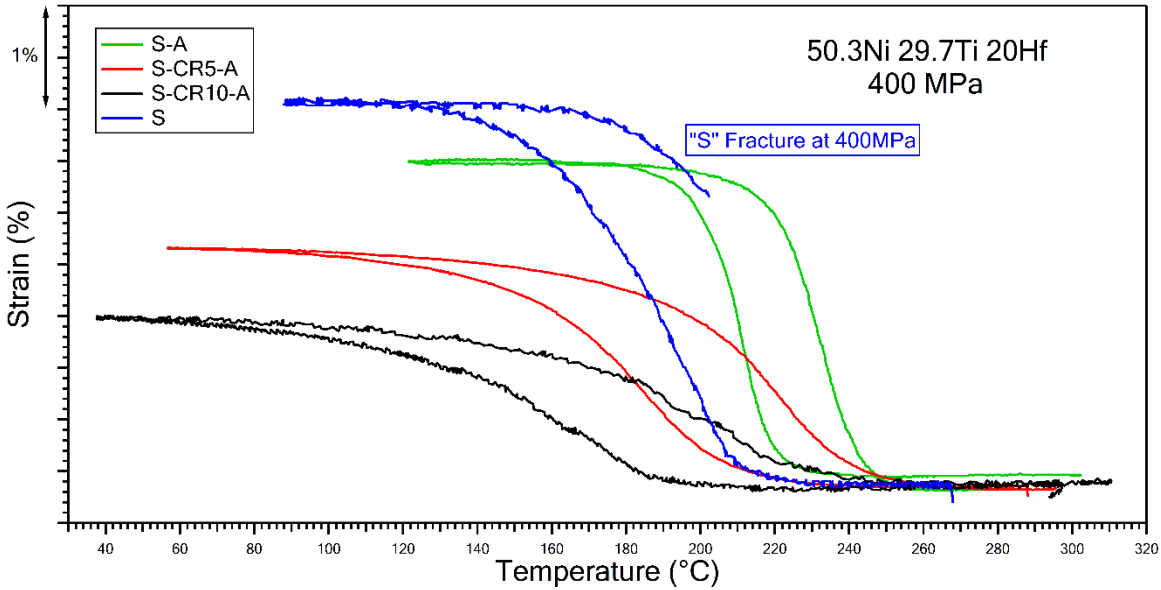

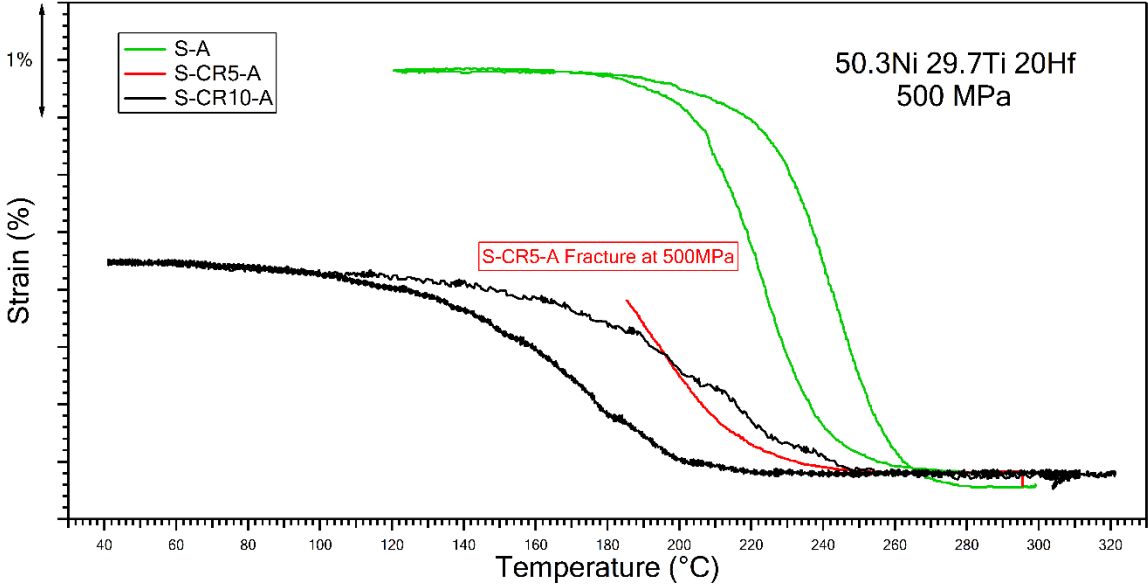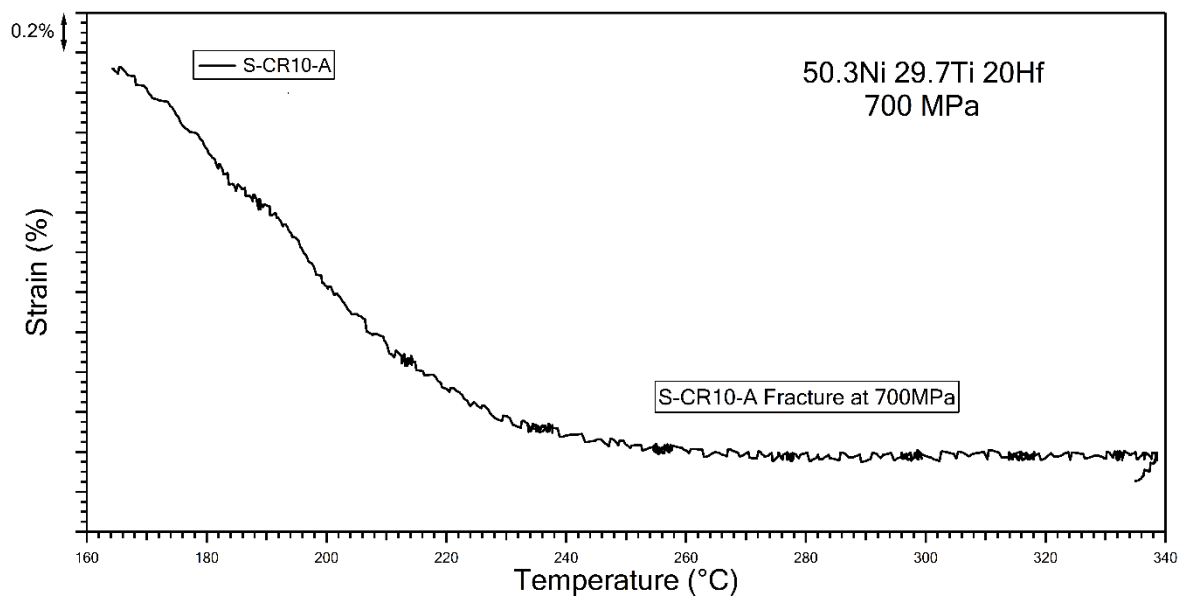Figure 4.2-8. Under 700 MPa applied stress, strain-temperature behaviour.

The actuation strains and the irrecoverable strains were obtained for all samples and were compared in Figure 4.2-9. It can be extracted that the actuation strains increase with the increment in applied stress. With respect to this graph, the actuation strains of cold-rolled samples are lower than that of S and S-A samples. The actuation strains diminish with the growth of deformation rate. This behavior can be explained with the increment in strength of samples which applied cold rolling. The critical stress for martensite phase transformation in cold rolled and aged samples must be greater. Because the greater stress levels should be required to obtain greater actuation strains. Additionally, cold rolling may also induce texture which leads to observe less actuation strain values. The texture effect on actuation strain value has already been argued for NiTi binary alloy for texture [54].

Figure 4.2-9 shows that, the irrecoverable strain values of all samples were very small for each stress magnitude since NiTiHf alloys are not only HTSMAs but also high strength SMAs. Therefore, irrecoverable strain is not noticeable in all samples due to the resistance to plastic deformation. The irrecoverable strain values were observed under 200 MPa and then diminished down to almost zero.
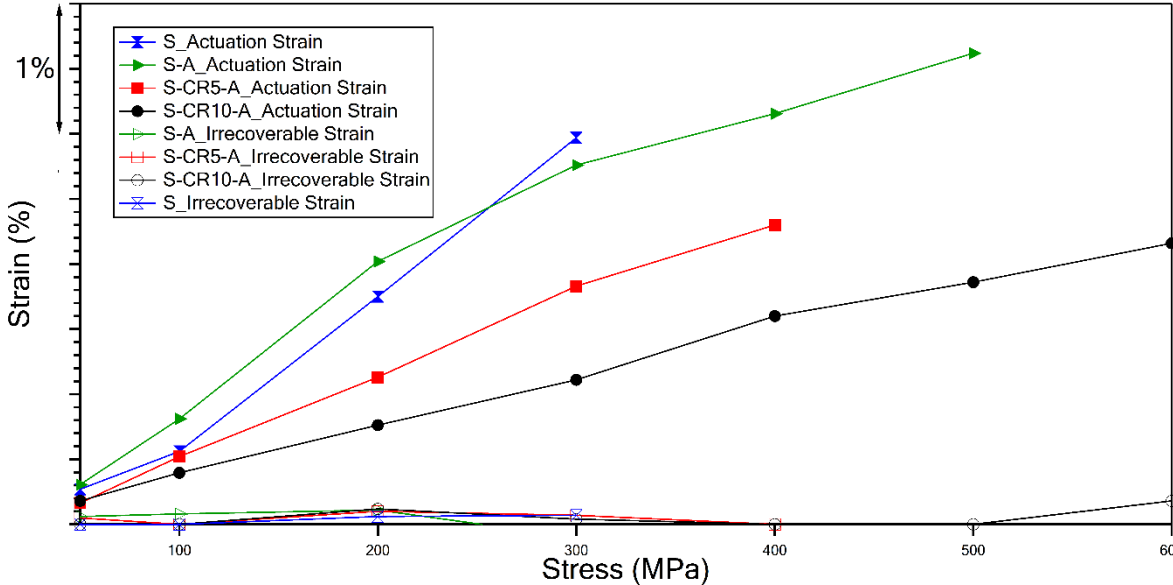
Figure 4.2-9. Actuation strains and irrecoverable strains of all samples.

The figure 4.2-10 demonstrates the thermal hysteresis data of all samples for each applied stress. S-A sample has the lowest thermal hysteresis, while the cold rolled samples show the largest thermal hysteresis as shown in Figure 4.2-10. The cold rolled samples have similar behavior after 200 MPa applied stress. The unexpected thermal hysteresis result of S-CR5-A and S-CR10-A under 100 MPa is dedicated to the instability of the temperature measurement during running the experiment.
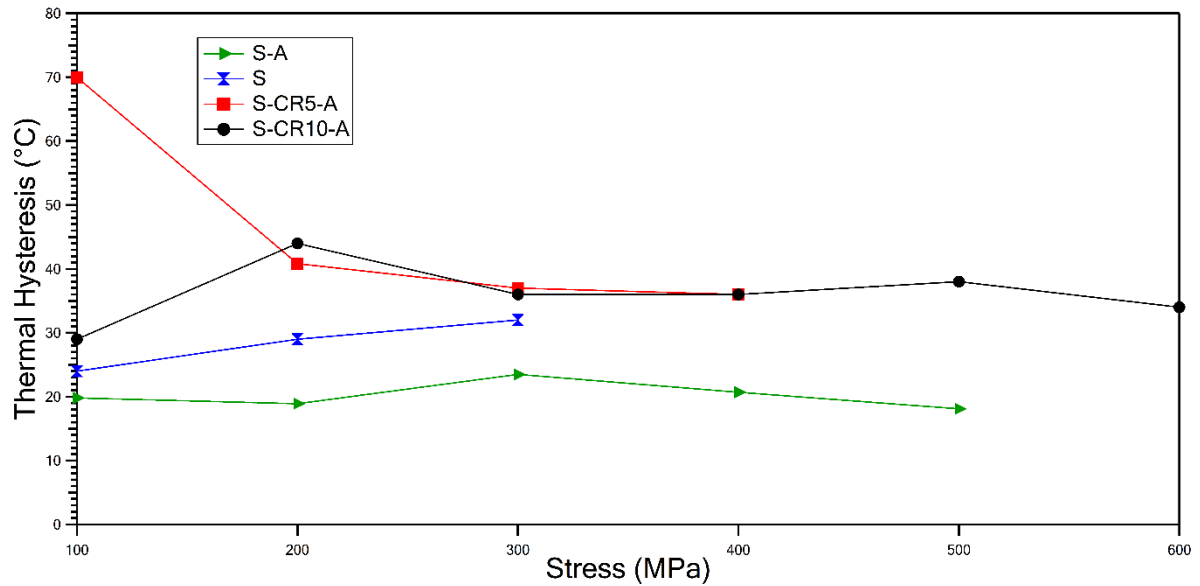
Figure 4.2-10.   The thermal hysteresis evolution of all samples.

Figure 4.2-11 shows that the Ms temperatures of S-A, S-CR5-A and S-CR10-A for each stress level from 0 MPa to 500 MPa. M_s temperature values under no load were obtained from DSC experiments and combined with M_s temperature values which are collected from isobaric heating-cooling tests. It is obvious that the M_s temperatures diminish with the amount of the cold rolling percentage.
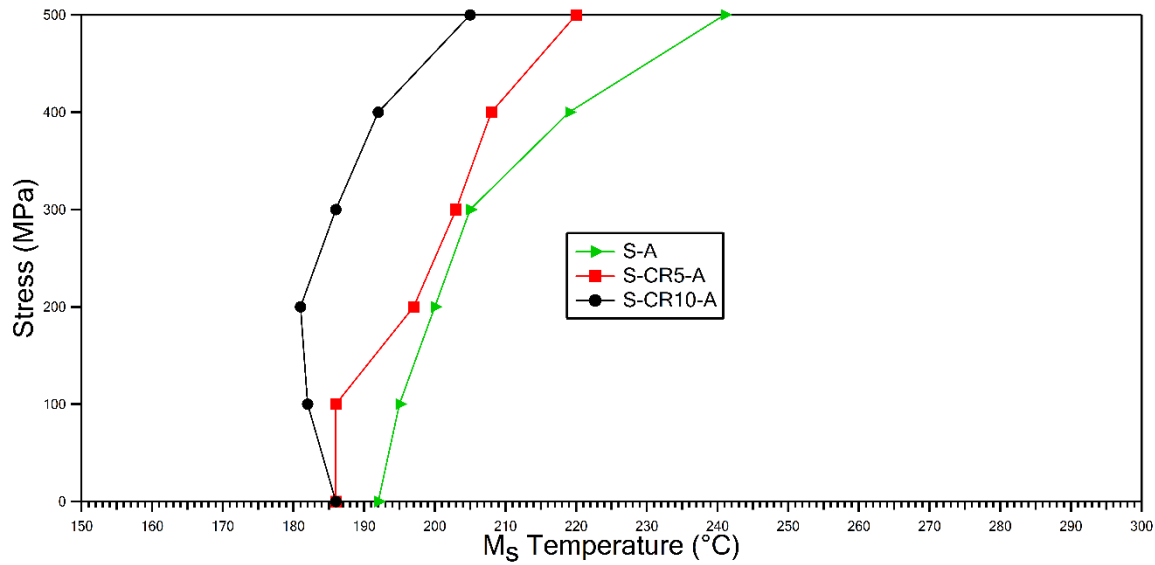
Figure 4.2-11.   The martensite start temperatures of S-A, S-CR5-A and S-CR10-A for each stress levels from 0 Mpa to 500 MPa.

4.3. Functional Fatigue Experiments

Functional fatigue (FF) tests were performed under 200 MPa stress. This magnitude is set as threshold level. Because the irrecoverable strain were not observed in 200 MPa stress during load-biased heating-cooling tests. To specify upper cycle temperature (UCT), the behavior of the sample was observed during the first cycle. UCT is the temperature which should be sufficient to achieve martensite to austenite phase transformations completely. The samples have various dislocations and imperfections, especially after cold rolling operation. So, the UCT was set after the observation of first cycles. On the other hand, the dislocations accumulate in the matrix during fatigue experiments. Therefore, the transformation temperatures to achieve the full transformation increase since the dislocation density increase. Because, more overheating is required to overcome the dislocation barriers to phase transformation. UCT was set by considering these effects. As mentioned in section 2.4, it is explained that while the UCT increase, the actuation strain also increases. It causes early failure since UCT increase leads more expansion and contraction of cracks [23]. However, this study did not focus on the effect of UCT. The aim of this study was the effect of cold rolling on the functional fatigue life of $Ni_{50.3}Ti_{29.7}Hf_{20}$ HTSMA. Thus, the FF tests were conducted for S, S-CR5-A and S-CR10-A samples.

28

The graph shown in Figure 4.3-1 presents the strain-temperature behaviour of solutionized (S) sample. The failure was occurred after 2802 cycle. The shape memory properties stabilize and the shape memory behavior of the sample decreases throughout the cycles. It means that the actuation strain of the sample decreases.
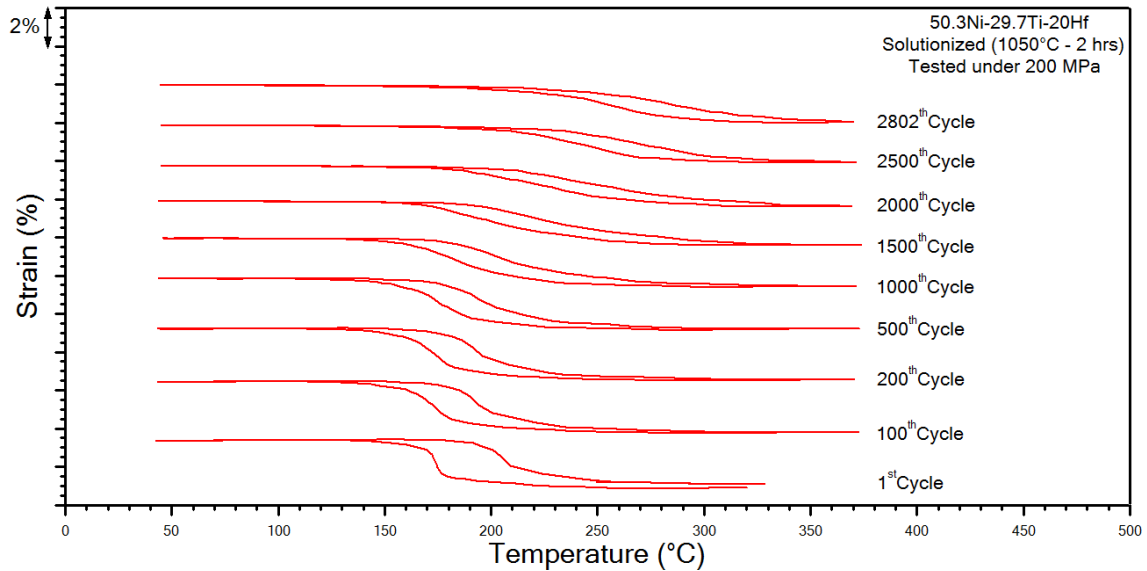
Figure 4.3-1. The change in strain-temperature behaviour of solutionized (S) sample throughout the cycles.

As mentioned in previous paragraph, the actuation strain diminishes throughout the cycles. However, as shown in Figure 4.3-2, there is a rapid increase during the first 100 cycles. The reason of the irrecoverable strain is the plastic deformation caused by the first applied load. After the first cycle, the actuation strain decreases until failure as expected. The actuation strain of the sample is 2.33% in the first cycle and 1.95% in the last cycle.
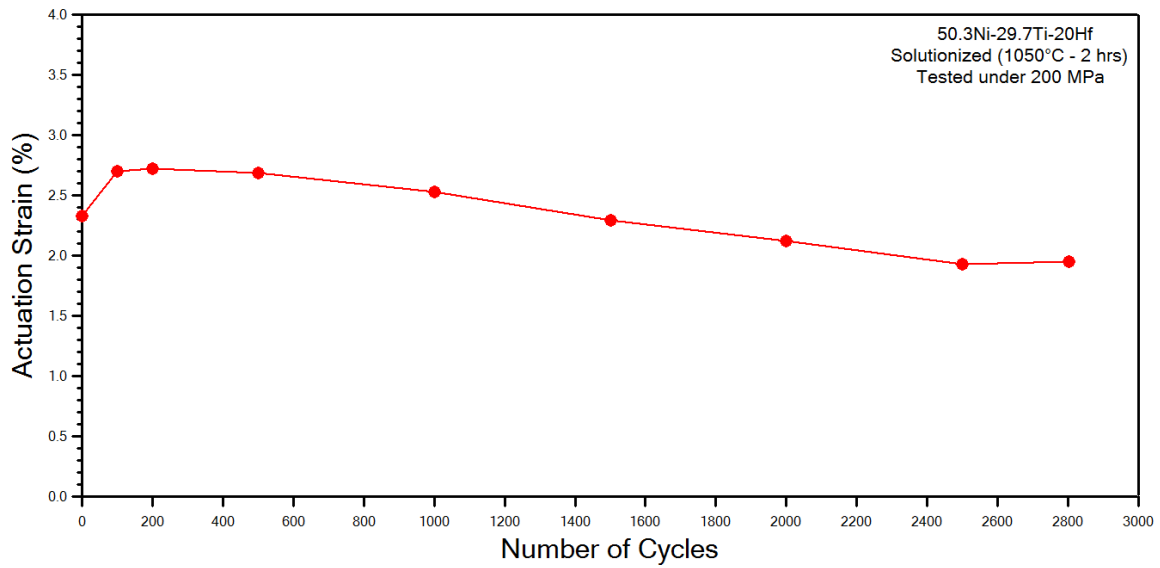
Figure 4.3-2. The change in actuation strain of solutionized (S) sample throughout the cycles.

Figure 4.3-3 exhibits the change in TTs throughout the cycles for solutionized (S) sample. It is obvious that all TTs has an increasing trend because of accumulation of dislocations during transformations with number of cycles. The transformation temperature values with respect to cycles are listed with Table 4.3-1. It can be seen that the accumulated dislocations effect the M_s and A_f temperatures more than that of M_f and A_s temperatures.
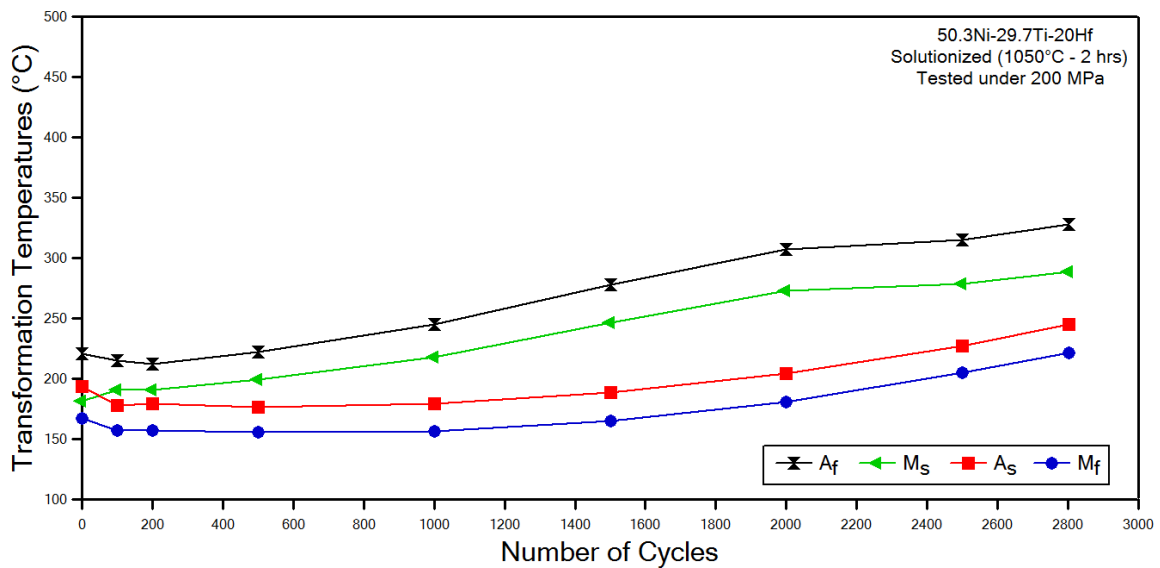
Figure 4.3-3. The change in TTs of solutionized (S) sample throughout the cycles.

Table 4.3-1.   Transformation temperature values of solutionized (S) sample and the difference between the first cycle and the last cycle.

Cycle	Mf (˚C)	Ms (˚C)	As (˚C)	Af (˚C)
1	166.9	181.1	193.4	220.9
100	156.8	190.6	178.2	214.7
200	157.1	190.7	179.1	212.5
500	155.4	199.6	176.3	222.3
1000	156.2	217.8	179.5	245.1
1500	165.2	246.1	188.8	278.1
2000	180.4	272.8	204.2	307.2
2500	205.1	278.7	227.1	315
2802	221.1	288.9	244.7	328
Difference (˚C) (Last - First)	54.2	107.8	51.3	107.1

During actuation fatigue cycling, the remnant shape change which cannot be recovered throughout the cycles is accumulated. The increase in the strain of austenite phase represents the total irrecoverable strain in functional fatigue experiments. The irrecoverable strain determination is not easy from cooling-heating cycles of functional fatigue experiments like those that it was done for load-biased experiments since the applied stress is 200 MPa and the irrecoverable strain values are very small at each cycles. Therefore, the procedure which was shown in Figure 4.3-4 as followed to determine accumulated irrecoverable and actuation strain values.
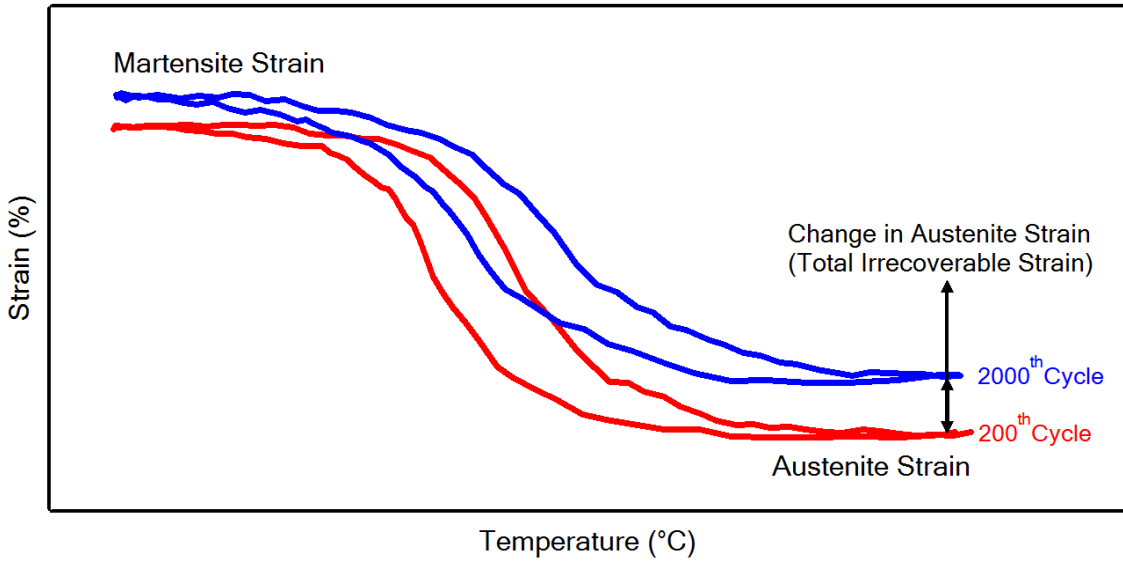
Figure 4.3-4.   Calculation of total irrecoverable strain during the fatigue cycles.

To trace the irrecoverable strain evolution of the sample, the strain vs. number of cycles data were generated in Figure 4.3-5. The blue line and the red line represents the strain levels at the end of the cooling and heating, respectively. The black line represents the actuation strain. The total irrecoverable strain is 2.2% for solutionized (S) sample after 2802 cycle.
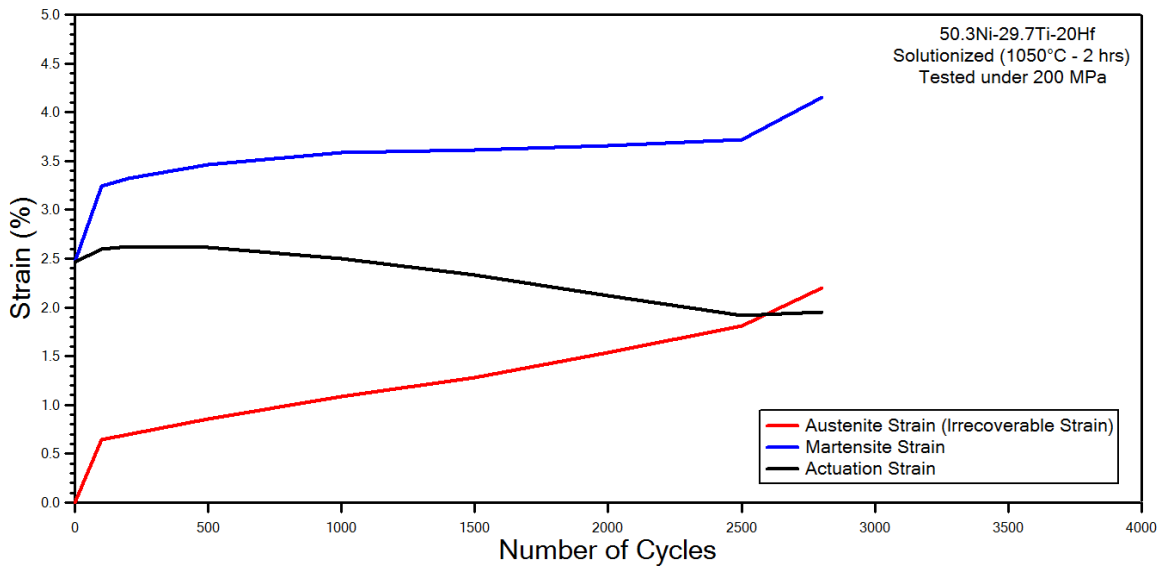
Figure 4.3-5.   The total austenite strain, the total martensite strain and actuation strain till fracture for solutionized (S) samples

Figure 4.3-6 shows the strain-temperature behaviour of S-CR5-A sample. The fracture was occurred after 5740 cycle.
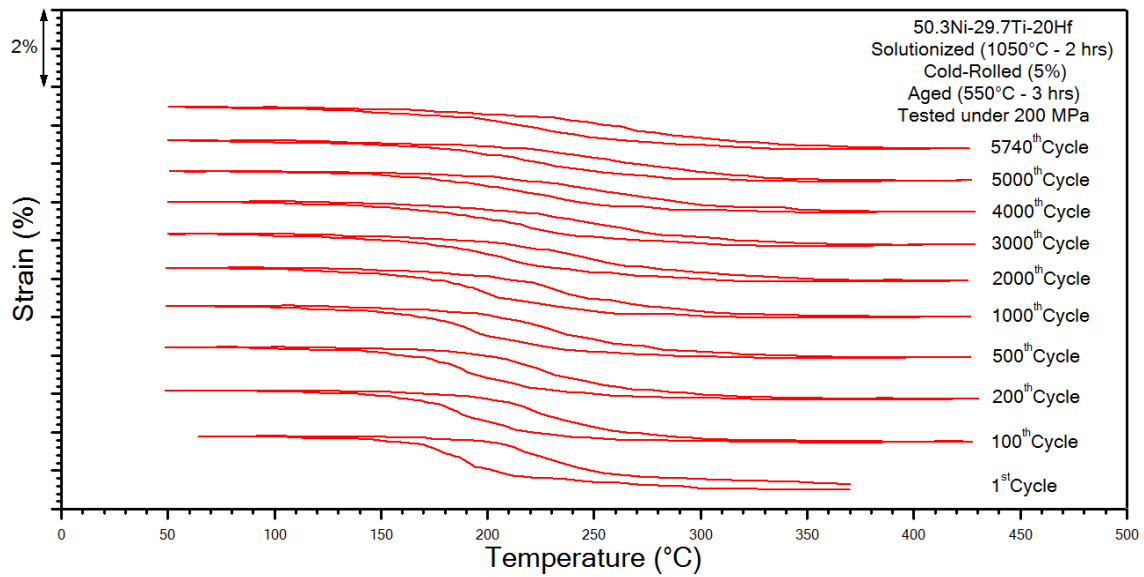
Figure 4.3-6. Strain-temperature behaviour of 5% cold-rolled (S-CR5-A) sample for different cycles.

As shown in Figure 4.3-6 and 4.3-7, it can be clearly seen that there is a small change in actuation strain throughout the cycles due to dislocation density of S-CR5-A sample. The cold rolling process induce very large amount of dislocations to the matrix. These dislocations enhance the strength of material and inhibit the formation of new dislocations during actuation fatigue cycling. Therefore, less dislocation accumulation stabilizes the shape memory properties such as the actuation strain throughout the fatigue cycles. The actuation strain was 1.25% in the first cycle and decreased to 1.10% after 5740th cycle.
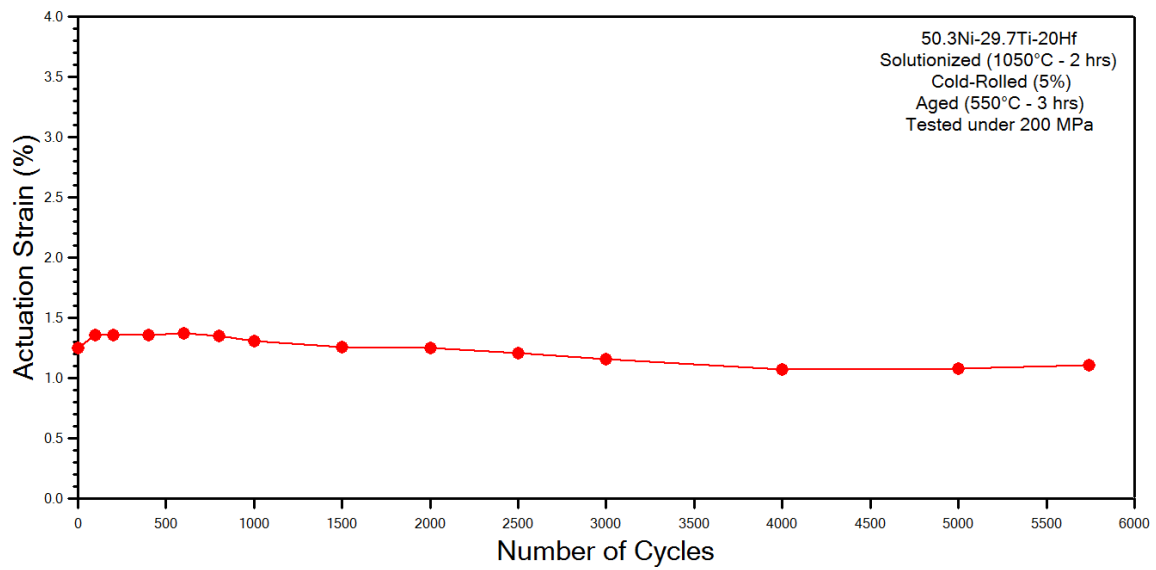
Figure 4.3-7. The change in actuation strain of 5% cold-rolled (S-CR5-A) sample throughout the cycles.

The change in TTs of S-CR5-A sample throughout the cycles were presented in Figure 4.3-8. It is clear that while Af and Ms temperatures increase approximately 60˚C throughout the fatigue cycles, there is no noticeable change in As and Mf temperatures until fracture occurs. The values of TTs of S-CR5-A sample were tabulated in Table 4.3-2. It can be noticed that the dislocation density provides a certain dimensional stability in terms of TTs and actuation strain.
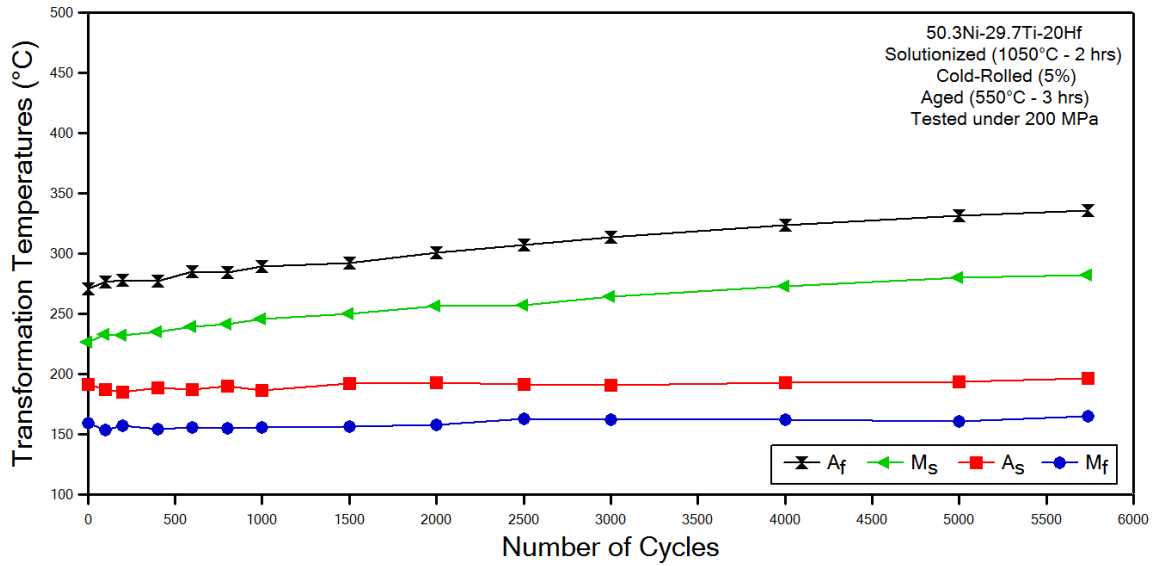
Figure 4.3-8. The change in TTs of 5% cold-rolled (S-CR5-A) sample throughout the cycles.

Table 4.3-2. Transformation temperature values of 5% cold-rolled (S-CR5-A) sample and the difference between the first cycle and the last cycle.

Cycle	Mf (°C)	Ms (°C)	As (°C)	Af (°C)
1	159.6	226.5	191.4	270.7
100	153.7	232.9	187.3	276.7
200	157.3	232.3	184.9	278.1
500	150.3	245	185.1	288.1
1000	156	245.6	186.6	289.5
1500	156.7	250	192.4	292.5
2000	158.2	256.7	192.7	300.7
2500	163	257.1	191.6	307.2
3000	162.3	264.2	190.9	313.8
4000	161.9	272.9	193.2	323.7
5000	161	280	193.8	331.7
5740	165.2	281.8	196.4	335.4
Difference (°C) (Last - First)	5.6	55.3	5	64.7

35

To observe the irrecoverable strain of the S-CR5-A sample, the strain vs. number of cycles data were drawn and shown in Figure 4.3-9. The total irrecoverable strain is 1.02% for S-CR5-A sample after 5740 cycle. The very large amount of dislocation blocks the dislocation formation together with the motion of the existent dislocations and enhance strength. It leads to improve the critical shear stress to slip. So, the total irrecoverable strain of S-CR5-A sample are low relatively lower than that of the solutionized (S) sample.
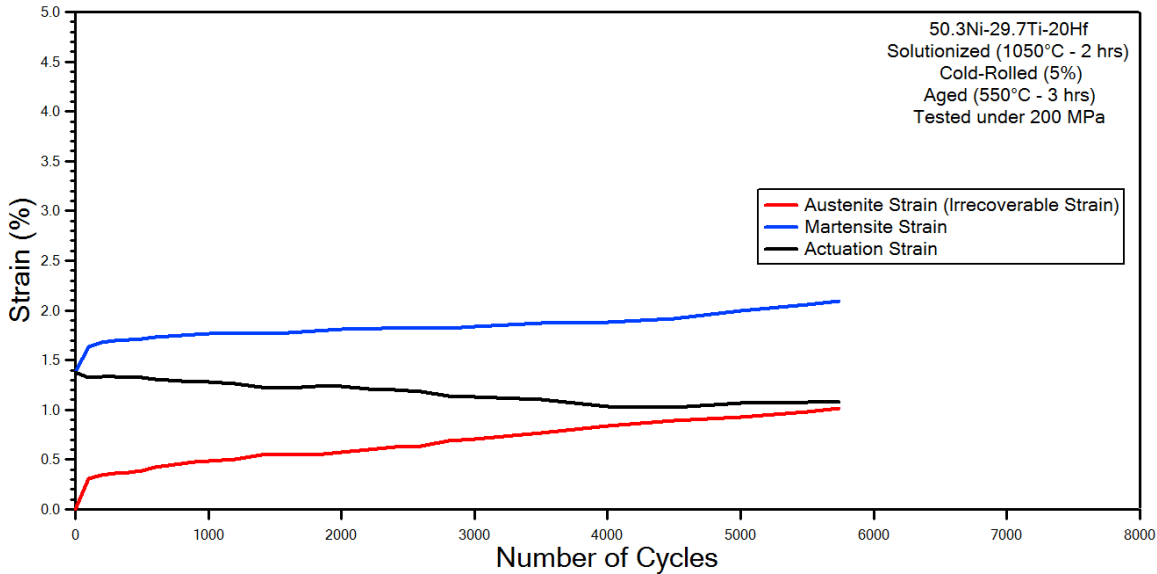
Figure 4.3-9.   The total austenite strain, the total martensite strain and actuation strain til fracture for 5% cold-rolled (S-CR5-A) sample.

Figure 4.3-10 exhibits the strain-temperature behaviour of S-CR10-A sample. The sample fractures after 3425th cycle. As mentioned before, the shape memory characteristics decrease with number of cycles because of accumulated dislocations through the cycles. It is also mentioned that the dislocation density increase with cold working inhibit the dislocation accumulation during the cooling-heating cycles. In matrix of S-CR10-A sample, the amount of dislocations which are induced with cold rolling increased intensively due to the increase in the rate of the cold rolling process.
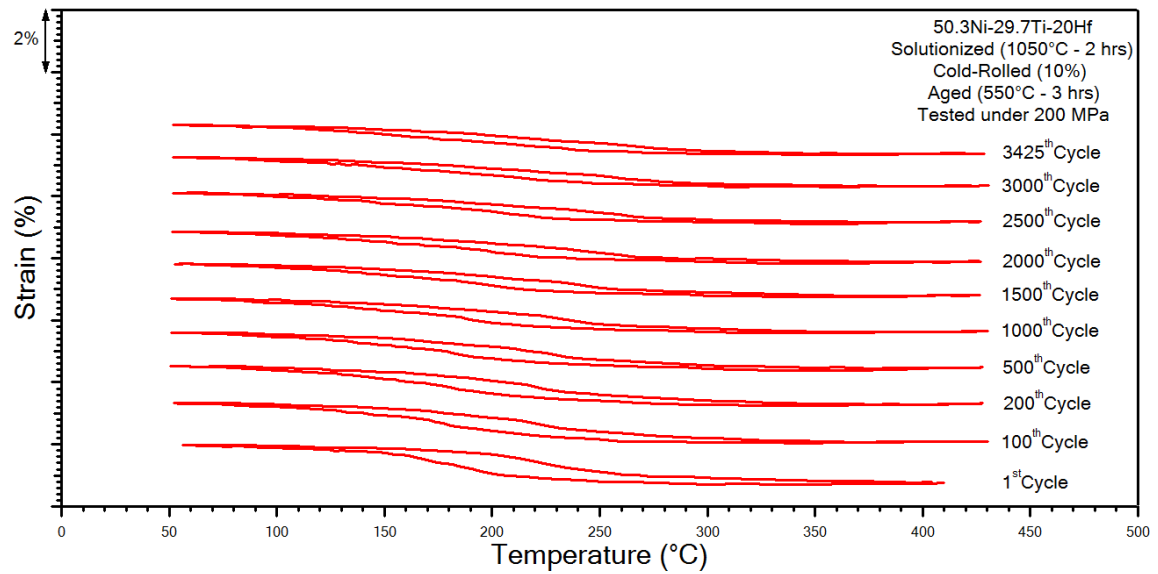
Figure 4.3-10.   Strain-temperature behaviour of 10% cold-rolled (S-CR10-A) sample for
different cycles.

Figure 4.3-11 exhibits the change in actuation strain of S-CR10-A sample. The actuation strain was 1.21% in the first cycle and diminished to 1.10% at the end of the 3425th cycle. There is a small decrease in actuation strain because of very intensive dislocation density which leads to cyclic stability as expected. Therefore, one could say that the increase in the cold rolling percentage decreases the magnitude of the actuation strain due to two reasons. First of all, texture may be induced with the cold rolling process. The texture that can be obtained with cold rolling of NiTi binary alloys led to observe the least transformation strain [55]. Secondly, dislocations block the boundaries of martensite and twins such that mobility of the twin boundaries decreases and thus the transforming volume decreases.
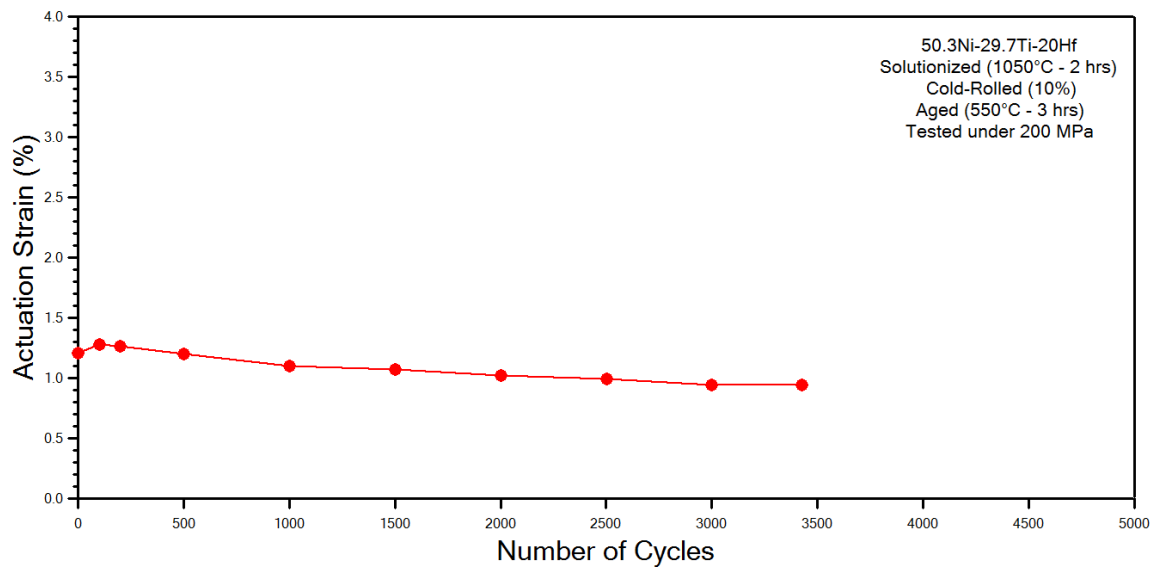
Figure 4.3-11.   The change in actuation strain of 10% cold-rolled (S-CR10-A) sample throughout the cycles.

Figure 4.3-12 represents the evolution of TTs of S-CR10-A sample throughout the cycles. Although the fracture occurred after 3425 cycle, the TTs of the first 1000 cycles were evaluated for S-CR10-A sample since the forward and reverse transformations had been completed in wide range. The slope of the transformation curve is not distinct such that the determination of the transformation temperatures is not possible by using the tangent method as shown in Figure 2-3. A_s and M_f temperatures slightly decrease while A_f and M_s temperatures slightly increase, during the first 100 cycles. There is no noticeable change in transformation temperatures after 100th cycle due to high dislocation density. The transformation temperature values were listed in Table 4.3-3. The small change in transformation temperatures can be observed numerically in Table 4.3-3.
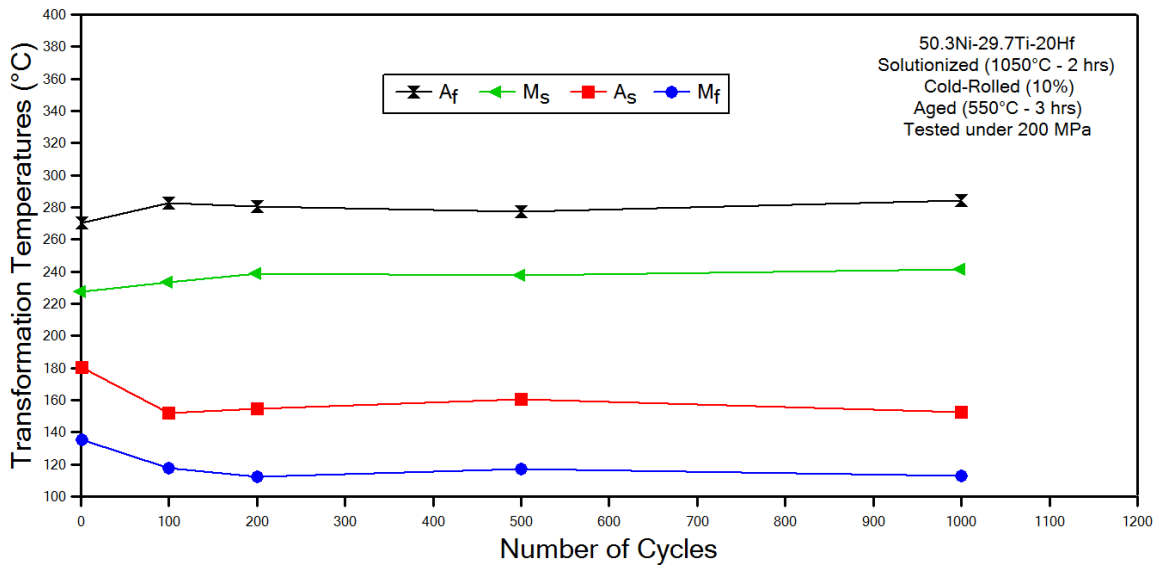
Figure 4.3-12.   Evolution of the TTs of 10% cold-rolled (S-CR10-A) sample throughout the cycles.

Table 4.3-3.   Transformation temperature values of 10% cold-rolled (S-CR10-A) sample and the difference between the first cycle and the 1000th cycle.

Cycle	Mf (°C)	Ms (°C)	As (°C)	Af (°C)
1	135.4	227.7	180.2	270.5
100	117.6	233.5	151.8	282.6
200	112.3	238.6	154.5	280.6
500	117	237.6	160.7	277.3
1000	112.8	241.6	152.4	284.3
Difference (°C) (1000th Cycle - First)	-22.6	13.9	-27.8	13.8

To observe the irrecoverable strain of the S-CR10-A sample, the strain vs. number of cycles data were drawn and shown in Figure 4.3-13. The total irrecoverable strain is 0.55% for this sample after 3425 cycle. The lowest irrecoverable strain was achieved with S-CR10-A sample and it proves that the growth in dislocation density improves critical shear stress to slip and enhances cyclic stability.

Figure 4.3-13. The total austenite strain, the total martensite strain and actuation strain till fracture for 10% cold-rolled (S-CR10-A) sample.

Figure 4.3-14 exhibits comparison of the S, S-CR5-A and S-CR10 samples in terms of the actuation strain throughout the fatigue cycles. It can be clearly compared that the actuation strain values decrease with the cold rolling extremely since the dislocations which are created with cold rolling prevent the martensite boundary movement such that the transforming volume decreases. Additionally, cold rolling may lead to the formation of texture and this texture may give the lowest actuation strain value. On the other hand, the cyclic stability of the alloy was improved with cold rolling process because of dislocation density.
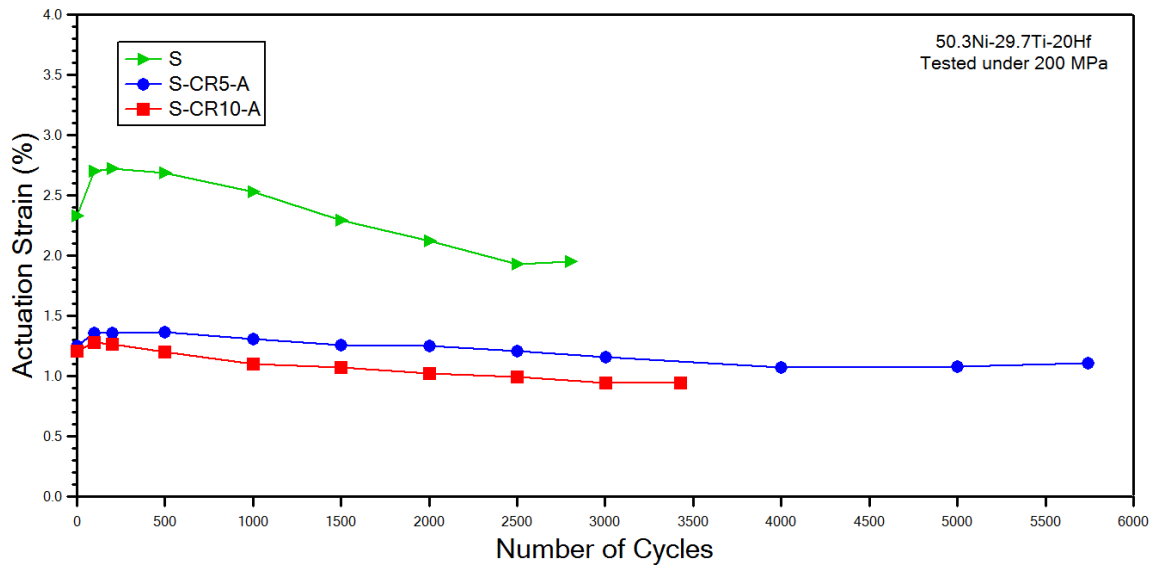
Figure 4.3-14. Comparison of actuation strain evolution throughout the cycles of S, S-CR5-A and S-CR10-A samples.

The comparison of the TTs were exhibited in Figure 4.3-15 and the differences of the TTs which were obtained from first cycle and last cycle were listed in Table 4.3-4. It is obvious that the TTs of the cold-rolled samples are more stable than the solutionized (S) sample. All the transformation temperatures of solutionized (S) sample change extremely during the fatigue cycles. While A_f and M_s temperatures of solutionized (S) sample are lower than that of the cold-rolled samples at the beginning, they become higher after 2000 cycle since the accumulation of dislocations causes an increase in TTs. The TTs of cold-rolled samples do not increase so much with the number of cycles due to the induced dislocations via cold rolling. It proves that the cold rolling process enhance the cyclic stability in TTs.
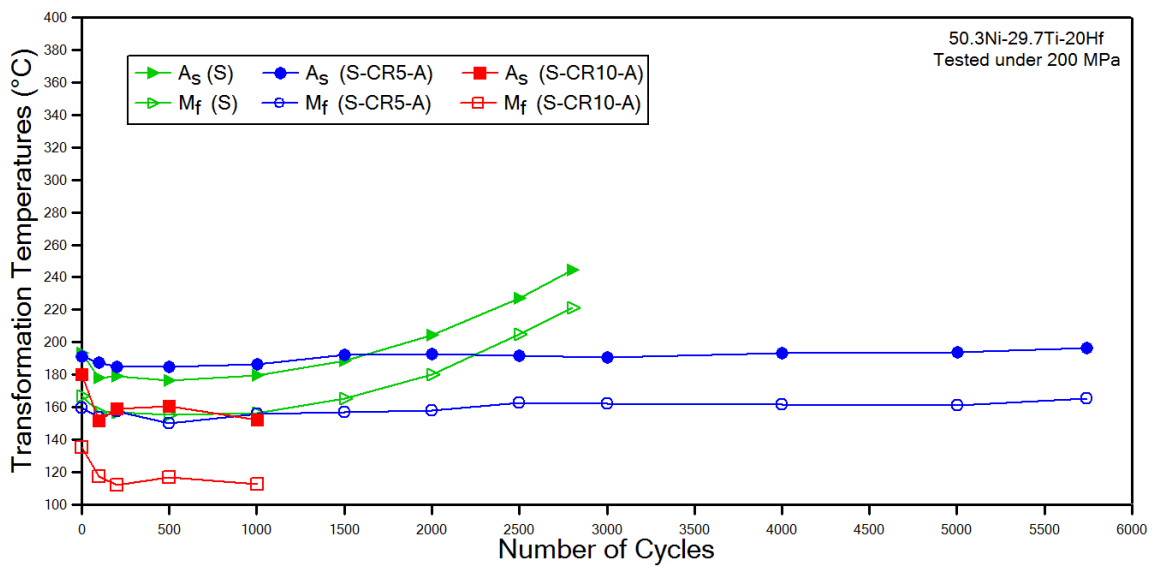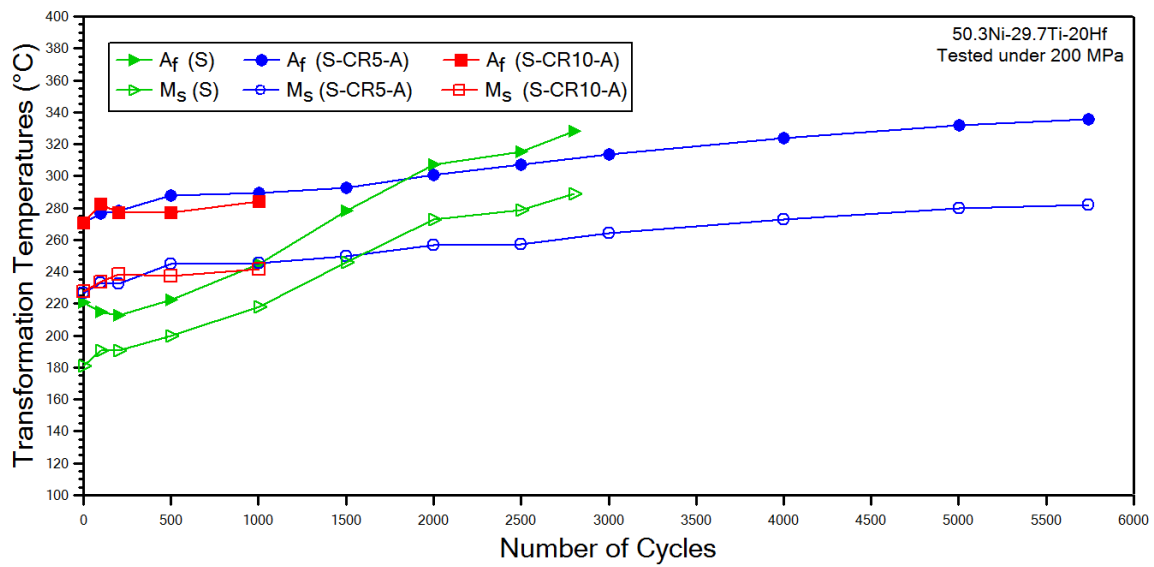
Figure 4.3-15. Comparison of the TTs evolution with throughout the cycles of S, S-CR5-A and S-CR10-A samples.

Table 4.3-4. The differences of TTs between first cycle and last cycle (1000th cycle for S-CR10-A).

Sample	Mf (˚C)	Ms (˚C)	As (˚C)	Af (˚C)
(S) Difference (˚C) (Last - First)	54.2	107.8	51.3	107.1
(S-CR5-A) Difference (˚C) (Last - First)	5.6	55.3	5	64.7
(S-CR10-A) Difference (˚C) (1000th Cycle - First)	-22.6	13.9	-27.8	13.8

Figure 4.3-16 shows the total strain changes of S, S-CR5-A and S-CR10-A samples. It can be seen that the cold rolling decrease the irrecoverable strains of the alloy besides the actuation strain and the total martensite strain.

Another intriguing finding is the diminishment in fatigue life of the samples with increment in cold rolling percentage. Although the strength of the alloy was enhanced with the cold rolling operation the fatigue life was diminished due to the increase in the formation of the crack with the cold rolling. NiTiHf alloys are not only high temperature shape memory alloys but also high strength alloys. Therefore, they can be called as hard to deform materials. 5 and 10% of cold rolling processes may lead to form more cracks and these cracks are the main reasons of earlier failure.
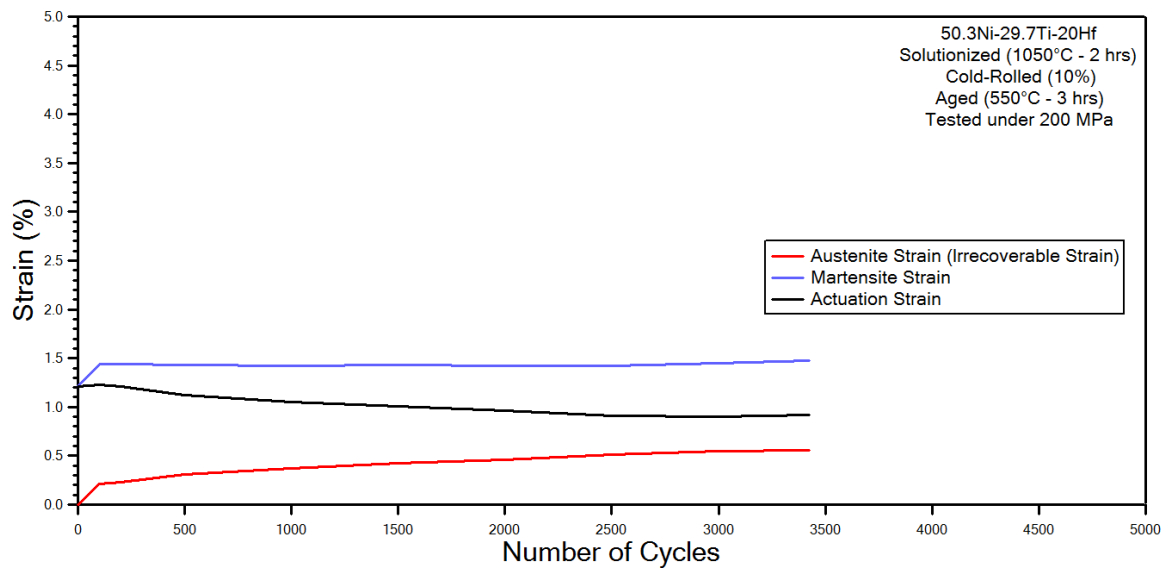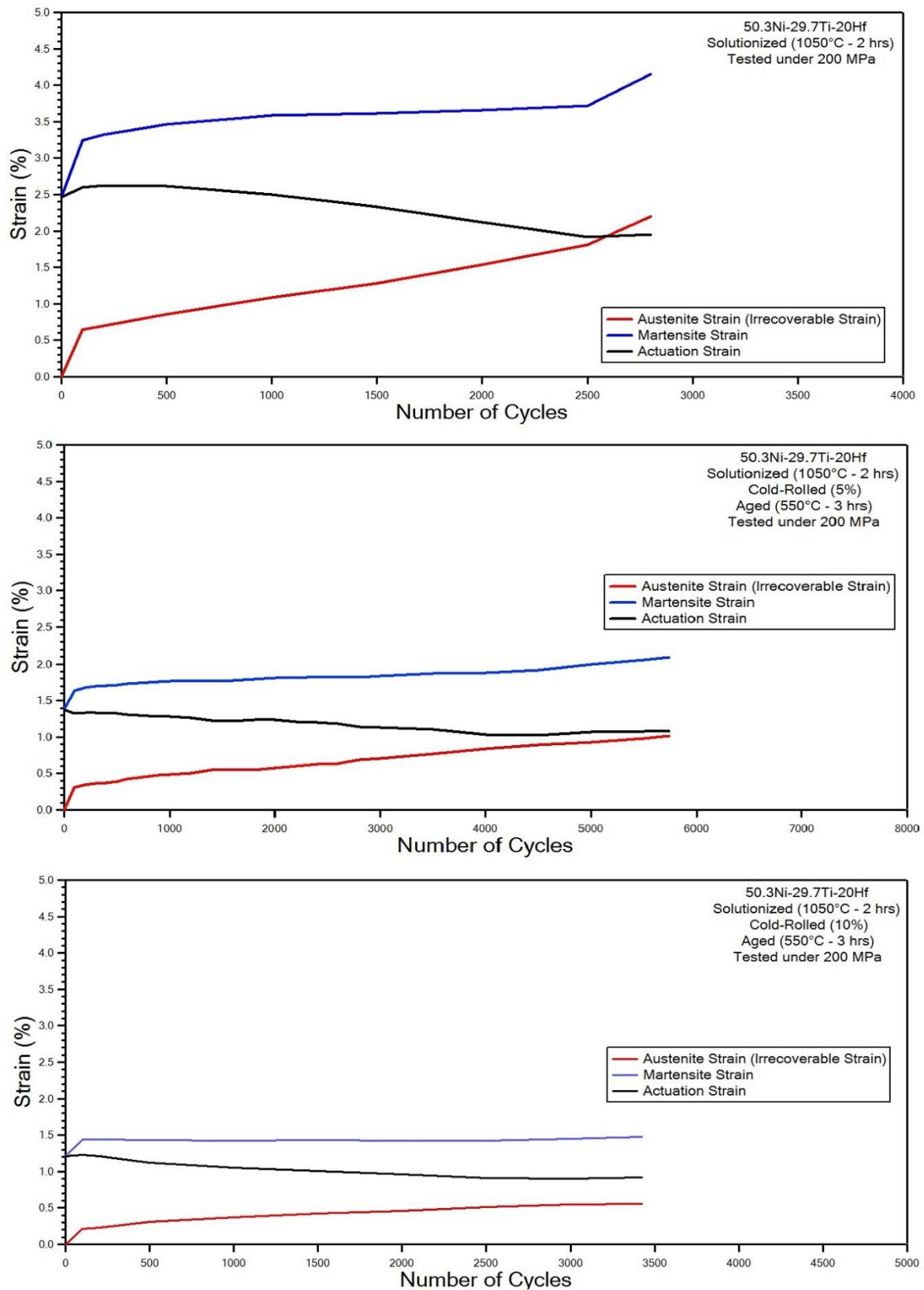
Figure 4.3-16. The total austenite strain, the total martensite strain and actuation strain till fracture for S, S-CR5-A and S-CR10-A samples.

5. CONCLUSION

The main conclusions which are gathered with evaluating all the aforementioned results are summarized below:

The results of the load-biased heating-cooling tests showed that the cold rolling process decreases the actuation strain. The actuation strains decrease with the increment of the percentage of cold rolling due to the texture formation or the decrease in the transforming volume. At the same time, these dislocations and the nano-precipitates which are formed via cold rolling and aging heat treatment block dislocation formation and improve strength of the alloy. Thus, the critical stress for phase transformation must be higher to obtain higher actuation strains. The another observation is that the irrecoverable strain of all samples were very low due to the high strength of NiTiHf HTSMAs and decreased further with the cold rolling and aging processes.

It is clear that the cold rolling process improves the cyclic stability of Ni50,3Ti29,7Hf20 HTSMAs from the point of actuation strain and TTs regarding the results of the functional fatigue experiments. The stability of the actuation strain values and the TTs was achieved with the growth in dislocation density via cold rolling and the nanoprecipitate formation via aging. In solutionized (S) sample, the dislocation density should be lower than that of the cold rolled samples and should not have nanoprecipitates. Martensite-austenite phase transformation leads to the formation of dislocations during the heating-cooling cycles. Plastic shape change may appear due to these dislocations which form during the cycles and thus irrecoverable strain magnitude increases. It is also important to mention that the fatigue life was diminished due to the increase in the crack formation with the cold rolling. NiTiHf alloys are not only HTSMAs but also high strength alloys such that it is very difficult to deform them. Cold rolling process leads to the formation of more cracks and these cracks can easily propagate during the functional fatigue heating-cooling cycles. Therefore, the functional fatigue life after cold rolling decreases.

This is the first study that investigates the effect of cold rolling with aging on the functional fatigue properties of Ni50,3Ti29,7Hf20 HTSMAs in the literature. With this study, it is proved that the cold rolling after aging process enhance the cyclic stability of Ni50,3Ti29,7Hf20 HTSMAs.

REFERENCES

[1]   K. Otsuka, X. Ren, Physical metallurgy of Ti-Ni-based shape memory alloys, Progress in Materials Science. 50 (2005) 511–678.

[2]   B. Kockar, I. Karaman, J.I. Kim, Y.I. Chumlyakov, J. Sharp, C.J. (Mike. Yu, Thermomechanical cyclic response of an ultrafine-grained NiTi shape memory alloy, Acta Materialia. 56 (2008) 3630–3646.

[3]   J. Ma, I. Karaman, R.D. Noebe, J. Ma, I. Karaman, R.D. Noebe, High temperature shape memory alloys High temperature shape memory alloys, International Materials Reviews. 55 (2010) 257–315.

[4]   B. Kockar, K.C. Atli, J. Ma, M. Haouaoui, I. Karaman, M. Nagasako, R. Kainuma, Role of severe plastic deformation on the cyclic reversibility of a Ti 50.3Ni33.7Pd16 high temperature shape memory alloy, Acta Materialia. 58 (2010) 6411–6420.

[5]   R. Santamarta, R. Arróyave, J. Pons, A. Evirgen, I. Karaman, H.E. Karaca, R.D. Noebe, TEM study of structural and microstructural characteristics of a precipitate phase in Ni-rich Ni-Ti-Hf and Ni-Ti-Zr shape memory alloys, Acta Materialia. 61 (2013) 6191–6206

[6]   A. Evirgen, I. Karaman, R.D. Noebe, R. Santamarta, J. Pons, Effect of precipitation on the microstructure and the shape memory response of the Ni50.3Ti29.7Zr20 high temperature shape memory alloy, Scripta Materialia. 69 (2013) 354–357.

[7]   G.S. Firstov, J. Van Humbeeck, Y.N. Koval, Comparison of high temperature shape memory behaviour for ZrCu-based, Ti-Ni-Zr and Ti-Ni-Hf alloys, Scripta Materialia. 50 (2004) 243–248.

[8]   G.S. Firstov, Y.N. Koval, J. Van Humbeeck, R. Portier, P. Vermaut, P. Ochin, Phase transformations in Zr-29.56 at.% Cu-19.85 at.% Ni melt-spun high-temperature shape memory alloy, Materials Science and Engineering A. 438–440 (2006) 816–820.

[9]   L. Patriarca, H. Sehitoglu, High-temperature superelasticity of Ni50.6Ti24.4Hf25.0 shape memory alloy, Scripta Materialia. 101 (2015) 12–15.

[10]   B. Kockar, I. Karaman, J.I. Kim, Y. Chumlyakov, A method to enhance cyclic reversibility of NiTiHf high temperature shape memory alloys, Scripta Materialia. 54 (2006) 2203–2208.

[11]   X.L. Meng, Y.F. Zheng, Z. Wang, L.C. Zhao, Shape memory properties of the Ti36Ni49Hf15 high temperature shape memory alloy, Materials Letters. 45 (2000) 128–132.

[12]   H.E. Karaca, E. Acar, H. Tobe, S.M. Saghaian, NiTiHf-based shape memory alloys, Materials Science and Technology (United Kingdom). 30 (2014) 1530–1544.

[13]   X.L. Meng, W. Cai, Y.D. Fu, Q.F. Li, J.X. Zhang, L.C. Zhao, Shape-memory behaviors in an aged Ni-rich TiNiHf high temperature shape-memory alloy, Intermetallics. 16 (2008) 698–705.

[14]   A. Evirgen, F. Basner, I. Karaman, R.D. Noebe, J. Pons, R. Santamarta, Effect of aging on the martensitic transformation characteristics of a Ni-Rich NiTiHf high temperature shape memory alloy, Functional Materials Letters. 5 (2012) 1–5.

[15]   D.R. Angst, P.E. Thoma, M.Y. Kao, The Effect of Hafnium Content on the Transformation Temperatures of Ni 49 Ti 51-x Hf x . Shape Memory Alloys , Journal de Physique IV. 05 (1995) C8-747-C8-752.

[16]   X.L. Meng, W. Cai, F. Chen, L.C. Zhao, Effect of aging on martensitic transformation and microstructure in Ni-rich TiNiHf shape memory alloy, Scripta Materialia. 54 (2006) 1599–1604.

[17]   A. Evirgen, I. Karaman, R. Santamarta, J. Pons, R.D. Noebe, Microstructural characterization and shape memory characteristics of the Ni50.3Ti34.7Hf15 shape memory alloy, Acta Materialia. 83 (2015) 48–60.

[18]   O. Benafan, A. Garg, R.D. Noebe, G.S. Bigelow, S.A. Padula, D.J. Gaydosh, N. Schell, J.H. Mabe, R. Vaidyanathan, Mechanical and functional behavior of a Ni-rich Ni50.3Ti 29.7Hf20 high temperature shape memory alloy, Intermetallics. 50 (2014) 94–107.

[19]   S.M. Saghaian, H.E. Karaca, M. Souri, A.S. Turabi, R.D. Noebe, Tensile shape memory behavior of Ni50.3Ti29.7Hf20 high temperature shape memory alloys, Materials and Design. 101 (2016) 340–345.

[20]   G.S. Bigelow, A. Garg, S.A. Padula, D.J. Gaydosh, R.D. Noebe, Load-biased shape-memory and superelastic properties of a precipitation strengthened high-temperature Ni50.3Ti29.7Hf20 alloy, Scripta Materialia. 64 (2011) 725–728.

[21]   H.H. Saygili, H.O. Tugrul, B. Kockar, Effect of Aging Heat Treatment on the High Cycle Fatigue Life of Ni50.3Ti29.7Hf20 High-Temperature Shape Memory Alloy, Shape Memory and Superelasticity. 5 (2019) 32–41.

[22]   H.E. Karaca, S.M. Saghaian, G. Ded, H. Tobe, B. Basaran, H.J. Maier, R.D. Noebe, Y.I. Chumlyakov, Effects of nanoprecipitation on the shape memory and material properties of an Ni-rich NiTiHf high temperature shape memory alloy, Acta Materialia. 61 (2013) 7422-7431

[23] O. Karakoc, C. Hayrettin, M. Bass, S.J. Wang, D. Canadinc, J.H. Mabe, D.C. Lagoudas, I. Karaman, Effects of upper cycle temperature on the actuation fatigue response of NiTiHf high temperature shape memory alloys, Acta Materialia. 138 (2017) 185–197.

[24] O. Karakoc, C. Hayrettin, D. Canadinc, I. Karaman, Role of applied stress level on the actuation fatigue behavior of NiTiHf high temperature shape memory alloys, Acta Materialia. 153 (2018) 156–168.

[25] N. Babacan, M. Bilal, C. Hayrettin, J. Liu, O. Benafan, I. Karaman, Effects of cold and warm rolling on the shape memory response of Ni50Ti30Hf20 high-temperature shape memory alloy, Acta Materialia. 157 (2018) 228–244.

[26] C.P. Frick, A.M. Ortega, J. Tyber, A.E.M. Maksound, H.J. Maier, Y. Liu, K. Gall, Thermal processing of polycrystalline NiTi shape memory alloys, Materials Science and Engineering A. 405 (2005) 34–49.

[27] K. Gall, J. Tyber, G. Wilkesanders, S.W. Robertson, R.O. Ritchie, H.J. Maier, Effect of microstructure on the fatigue of hot-rolled and cold-drawn NiTi shape memory alloys, Materials Science and Engineering A. 486 (2008) 389–403.

[28] D. Treppmann, E. Hornbogen, On the influence of thermomechanical treatments on shape memory alloys, Journal De Physique. IV : JP. 7 (1997) 211–220.

[29] H.O. Tugrul, H.H. Saygili, M.S. Velipasaoglu, B. Kockar, Comparison of the transformation behavior of cold rolling with aging and hot extrusion with aging processed Ni 50.3 Ti 29.7 Hf 20 high temperature shape memory alloy , Smart Materials and Structures. 28 (2019) 105029.

[30] Duerig TW, Melton KN, Stöckel D, Wayman CM. Engineering Aspects of Shape Memory Alloys. Boston: Butterworth-Heinemann Ltd; 1990.

[31] Funakubo H. Shape Memory Alloys. Amsterdam: Gordon & Breach Publishing Group; 1987.

[32] Lagoudas DC. Shape Memory Alloys: Modeling and Engineering Applications. United States: Springer; 2008.

[33] W. Abuzaid, H. Sehitoglu, Functional fatigue of Ni50.3Ti25Hf24.7 – Heterogeneities and evolution of local transformation strains, Materials Science and Engineering A. 696 (2017) 482–492.

[34] Pops H, Massalski TB. Trans AIME 1964;230:1662.

[35] R. Dasgupta, A look into Cu-based shape memory alloys: Present scenario and future prospects, Journal of Materials Research. 29 (2014) 1681–1698.

[36] S. Miyazaki, T. Kawai, K. Otsuka, Study of Fracture in Cu-Al-Ni Shape Memory Bicrystals., Journal de Physique (Paris), Colloque, 1982.

[37] Y. Sutou, T. Omori, J.J. Wang, R. Kainuma, K. Ishida, Characteristics of Cu-Al-Mn-based shape memory alloys and their applications, Materials Science and Engineering A. 378 (2004) 278–282.

[38] Araki, Y. et al., Potential of superelastic Cu–Al–Mn alloy bars for seismic applications, vol. 40. (2011).

[39] T. Maruyama, H. Kubo, Ferrous (Fe-based) shape memory alloys (SMAs): properties, processing and applications, Shape Memory and Superelastic Alloys. (2011) 141–159.

[40] C. Lagoudas, D., Shape memory alloys. Modeling and engineering applications. Papers based on the presentations at the 1st annual workshop on multifunctional nanomaterials, Red River, NM, USA, March 13–16, 2006, vol. 1. (2008).

[41] J. Khalil-Allafi, A. Dlouhy, G. Eggeler, Ni4Ti3-precipitation during aging of NiTi shape memory alloys and its influence on martensitic phase transformations, Acta Materialia. 50 (2002) 4255–4274.

[42] A. Radi, J. Khalil-Allafi, M.R. Etminanfar, S. Pourbabak, D. Schryvers, B. Amin-Ahmadi, Influence of stress aging process on variants of nano-Ni4Ti3 precipitates and martensitic transformation temperatures in NiTi shape memory alloy, Materials and Design. 142 (2018) 93-100.

[43] Brno, D. H., On the precipitation in NiTi based shape memory alloys, no. April 2005, (2005).

[44] S. Miyazaki, Y. Ohmi, K. Otsuka, Y. Suzuki, Characteristics of Deformation and Transformation Pseudoelasticity in Ti-Ni Alloys., Journal de Physique (Paris), Colloque. 43 (1982).

[45] A.N. Bucsek, G.A. Hudish, G.S. Bigelow, R.D. Noebe, A.P. Stebner, Composition, Compatibility, and the Functional Performances of Ternary NiTiX High-Temperature Shape Memory Alloys, Shape Memory and Superelasticity. 2 (2016) 62–79.

[46] H. Sehitoglu, Y. Wu, L. Patriarca, Shape memory functionality under multi-cycles in NiTiHf, Scripta Materialia. 129 (2017) 11–15.

[47] P.L. Potapov, A. V. Shelyakov, A.A. Gulyaev, E.L. Svistunova, N.M. Matveeva, D. Hodgson, Effect of Hf on the structure of Ni-Ti martensitic alloys, Materials Letters. 32 (1997) 247–250.

[48] S. Besseghini, E. Villa, A. Tuissi, Ni-Ti-Hf shape memory alloy: Effect of aging and thermal cycling, Materials Science and Engineering A. 273–275 (1999) 390–394.

[49] O. Karakoc, C. Hayrettin, A. Evirgen, R. Santamarta, D. Canadinc, R.W. Wheeler, S.J. Wang, D.C. Lagoudas, I. Karaman, Role of microstructure on the actuation fatigue performance of Ni-Rich NiTiHf high temperature shape memory alloys, Acta Materialia. 175 (2019) 107-120.

[50] S. Miyazaki, Y. Igo, K. Otsuka, Effect of thermal cycling on the transformation temperatures of TiNi alloys, Acta Metallurgica. 34 (1986) 2045–2051.

[51] J.M. Legresy, G.M. Raynaud, Formation of a TiNi shape memory alloy, Journal de Physique IV. 1 (1991) 241–246.

[52] Aydogmus, T., Processing and characterization of porous titanium nickel shape memory alloys, PhD Thesis, Graduate School of Natural and Applied Sciences of Middle East Technical University, Ankara, 2010.

[53] Saygili H.H., The Development of a fatigue test machine to investigate the functional fatigue life of high temperature shape memory alloys and the determination of the functional fatigue life of these alloys, MSc Thesis, Graduate School of Science and Engineering of Hacettepe University, Ankara, 2018.

[54] K. Gall, H.J. Maier, Cyclic deformation mechanisms in precipitated NiTi shape memory alloys, Acta Materialia. 50 (2002) 4643–4657.

[55] K. Kitamura, S. Miyazaki, H. Iwai, M. Kohl, Effect of rolling reduction on the deformation texture and anisotropy of transformation strain in Ti-50.2at.%Ni thin plates, Materials Science and Engineering A. 273–275 (1999) 758–762.

Comparison of the transformation behavior of cold rolling with aging and hot extrusion with aging processed Ni$_{50.3}$Ti$_{29.7}$Hf$_{20}$ high temperature shape memory alloy

H Onat Tugrul[1], **Hasan H Saygili**[1,2], **Mustafa S Velipasaoglu**[1] **and Benat Kockar**[1]

[1] Hacettepe University, Mechanical Engineering Department, 06800, Beytepe, Ankara, Turkey
[2] Turkish Aerospace Industries Inc., Helicopter Conceptual Design, Kahramankazan 06980, Ankara, Turkey

E-mail: benat@hacettepe.edu.tr

Abstract

Among NiTiHf high temperature shape memory alloys, nickel rich ternary Ni$_{50.3}$Ti$_{29.7}$Hf$_{20}$ (at%) alloy has been studied extensively and found to be promising for high temperature applications especially in aerospace industry. NiTiHf alloys have very high strength and transformation temperatures (TTs) proportional to their hafnium percentage. Therefore, these alloys are accepted as a hard to deform material. Hot extrusion at 900 °C and solutionizing at 1050 °C-1100 °C treatments have been generally used in literature for the homogenization of the cast microstructure and chemistry and thus, the strength of the material eventually increases. In this study, one set of the as cast Ni$_{50.3}$Ti$_{29.7}$Hf$_{20}$ alloy was hot extruded at 900 °C and then aged at 550 °C for 3 h and the other set was solutionized at 1050 °C for 2 h, cold rolled for 10% at room temperature and then aged at 550 °C for 3 h. The TTs of the hot extruded, hot extruded and aged, solutionized, solutionized-cold rolled and aged samples were measured using DSC and heating-cooling experiments under increasing stress magnitudes starting from 100 MPa and increasing up to 600 MPa were conducted on all thermal and thermo-mechanically treated samples in order to compare the shape memory characteristics such as actuation strain, irrecoverable strain and TTs. The samples which were hot extruded and aged and solutionized-cold rolled and aged showed very high dimensional stability with no irrecoverable strain values up to 500 MPa. However, the actuation strain magnitudes of the cold rolled with aging processed sample were half of the actuation strain values of the sample which was hot extruded and aging treated. Additionally, higher undercooling and overheating were necessary to achieve full transformation in the cold worked samples. These results might be due to the very high dislocation density and texture formation which was induced during cold rolling process.

Keywords: NiTiHf, precipitation, cold rolling, load biased

(Some figures may appear in colour only in the online journal)

1. Introduction

Ni–Ti alloys are the most promising shape memory alloys (SMAs) due to their high strength and good cyclic stability properties. However, their transformation temperatures (TTs) which are lower than 100 °C limit their usage for most of the high temperature aerospace applications. Adding a ternary alloying element such as Au, Pt, Pd, Zr and Hf to Ni–Ti based SMAs is the method to achieve high TTs [1–4]. Au, Pt and Pd are not suitable since they are relatively more expensive than

that of Zr and Hf. Zr has a high oxygen affinity, thus makes the alloy brittle. Therefore, Hf would be the better choice in order produce high temperature NiTi based SMAs. Additionally, higher actuation strains can be achieved by the addition of Hf instead of Zr [5].

In Ni-rich NiTi and NiTiHf high temperature shape memory alloys (HTSMAs), micro and nano-scale precipitates can be formed via aging and these precipitates affect chemical and mechanical properties of the alloy. An increase in critical stress for slip such that huge stress levels can be applied to obtain higher actuation strain with the formation of nano-scale precipitates and this is the effect of precipitates to the mechanical properties of the alloy [6]. Formation of these precipitates also increases the TTs with the decrease of Ni content in the matrix which can be called as the effect of precipitates on the chemical properties of the alloy [7].

Up to now, researchers work on the aging effect on the actuation properties and the cyclic stability of Ni-rich $Ni_{50.3}Ti_{29.7}Hf_{20}$ alloy with typical formation of nano-precipitates in the matrix [8–13]. Different research studies have been dedicated to the microstructural investigation of precipitate size as well as the twinning formation in Ni-rich NiTiHf alloys [6, 8, 10]. Addition to the microstructural investigations, Karaca and his co-workers showed the aging effect via running load-biased heating-cooling experiments and revealed that aging at 550 °C for 3 h led to an increase in the strength of the material and a decrease in the plastic deformation during martensite–austenite tranformation under constant stress magnitudes [11]. Moreover, Karaman's group investigated the cyclic stability of this Ni-rich alloy via running functional fatigue experiments [14, 15]. They showed the effect of upper cycle temperature and the applied stress magnitude to the functional fatigue life and stated that the increase in upper cycle temperature and the applied stress magnitude led to a decrease in the number of cycles during fatigue experiments. It has been also shown that the functional fatigue life of $Ni_{50.3}Ti_{29.7}Hf_{20}$ can be enhanced by 3 times via conducting aging treatment at 550 °C for 3 h due to the formation of nano-precipitates [16]. $Ni_{50.3}Ti_{29.7}Hf_{20}$ alloy used in the aforementioned studies were hot extruded after casting to improve the chemical and microstructural homogenity before the aging heat treatment. Karaman's group has recently worked on $Ni_{50}Ti_{30}Hf_{20}$ near equiatomic HTSMAs and demonstrated the effect of cold rolling and subsequent annealing effect on the TTs by conducting stress free heating-cooling cycles and on the transformation and irrecoverable strain magnitudes by conducting load-biased heating cooling experiments [17]. Up to our best knowledge, there has been no study on the effect of cold rolling and subsequent aging process to the TTs and to the actuation and irrecoverable strain levels of Ni-rich $Ni_{50.3}Ti_{29.7}Hf_{20}$ alloy. Previous studies on $Ni_{50.3}Ti_{29.7}Hf_{20}$ HTSMA have shown that the TTs of this alloy can be increased via aging for 3 h above 500 °C. Aging $Ni_{50.3}Ti_{29.7}Hf_{20}$ alloy at 550 °C for 3 h gives optimum results in the literature if the magnitude of the TTs and cyclic stability behaviors are considered. Additionally, it is also known that the cyclic stability of NiTi based alloys can be increased with the application of plastic deformation techniques such as

equal channel angular extrusion (ECAE) and/or cold rolling due to the decrease in the grain size and the increase in dislocation density as well as critical stress for slip [18–21]. For instance, Gall and his group worked on the effect of hot rolling, cold rolling and the subsequent heat treatments on the transformation properties of Ti-50.9at%Ni binary SMAs and concluded that the influence of dislocation density increase with thermo-mechanical processes to prevent the plastic flow is as similar as the influence of small coherent precipitates on preventing the plastic flow [19]. In another study, the pseudoelasticity behavior of polycrystalline Ti-50.9at%Ni alloy was examined to understand the effect of heat treatment after hot rolling and cold drawn processes to the cyclic stability and the crack growth with the number of cycles of this alloy [20]. It was observed that the resistance to cyclic degradation in the material which was hot rolled with 300 °C–1.5 h heat treated and cold drawn with 300 °C–1.5 h heat treated was excellent and the lowest resistance to the degradation was experienced in the cold drawn material due to the residual stresses induced during the cold deformation process [20]. Additionally, Karaman group investigated the effect of severe plastic deformation via ECAE and 30% cold drawing with 300 °C post annealing processes to the cyclic stability of near equiatomic NiTi alloy during the heating cooling under constant stress experiments [22]. In this study, ECAEd and cold drawn samples were heated and cooled under 100 and 200 MPa for 10 cycles. It was revealed that the recoverable strain values of the ECAEd and cold drawn samples were very stable throughout the cycles but the total irrecoverable strain values under 200 MPa of the cold rolled sample was higher than that of the ECAEd sample. However, both of the processes increased the cyclic stability of the near equiatomic NiTi alloy [22]. Miller and Lagoudas found that cold working with subsequent annealing processes increased the dimensional stability of NiTi binary alloys via observing less irrecoverable strain values during heating cooling under increasing constant stress cycles and they also stated that the dimensional stability increased further with the increase in cold working amount [23]. Therefore, it can be concluded from the aforementioned studies on NiTi alloys that the thermal and the thermomechanical processes increase the dimensional and TT stability of the NiTi based alloys due to the dislocation density increase with work hardening such that the mobility of the dislocations mitigates during thermal cycling which leads to the stability of the shape memory properties [24].

In this study, one set of $Ni_{50.3}Ti_{29.7}Hf_{20}$ alloy batch was hot extruded and then aged at 550 °C for 3 h and the other set was solutionized at 1050 °C for 2 h and then cold rolled for 10% at room temperature and then 550 °C for 3 h age treated as a final step. The main aim was to determine and to compare the transformation behavior of this alloy with two different thermo-mechanical processing conditions such as the actuation and irrecoverable strain, TTs thermal hysteresis magnitudes under increasing constant stress for actuator applications at high temperatures. This comparison was done to eliminate the hot extrusion step for easier processing since extruding the hard to deform materials such as NiTiHf at
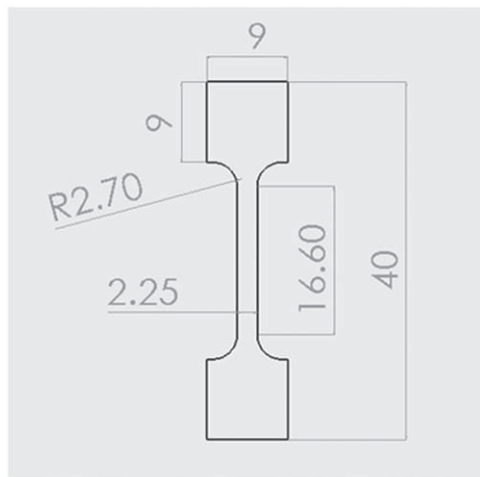
Figure 1. Tension test samples which were cut using WEDM (the dimensions were given in mm).

relatively higher temperatures generally requires expensive and complicated tools.

2. Experimental procedures

In this study, Ni, Ti and Hf elements having high purity levels were used to produce $Ni_{50.3}Ti_{29.7}Hf_{20}$ (at%) alloy via vacuum induction melting under high purity argon atmosphere. One set of the as cast $Ni_{50.3}Ti_{29.7}Hf_{20}$ alloy was sealed in a mild steel can and hot extruded at 900 °C with an area reduction of 4 to 1 and then aged at 550 °C for 3 h. The name conventions 'HE' and 'HE-A' will be used for hot extruded and hot extruded and aged samples, respectively throughout the text. The other set was solutionized at 1050 °C for 2 h. This set was also separated into 2 parts. One part was characterized in the as solutionized condition and the other part was cold rolled for 10% at room temperature and then aged at 550 °C for 3 h. Before solutionizing and aging heat treatments, the samples were wrapped in tantalum foil to diminish possible oxidation at relatively higher temperatures and both of the heat treatments were done in a vertical cylindrical furnace under high purity argon atmosphere and ended with water quenching. The name conventions 'S' and 'S-CR-A' will be used for the solutionized and solutionized-cold rolled and aged samples throughout the text for simplicity. The TTs of all samples were measured using differential scanning calorimetry (DSC) with a heating-cooling rate of 10 °C min⁻¹.

Dog bone shape tensile test samples which were used in load biased heating-cooling experiments with a gage length of 16.6 mm, a width of 2.25 mm and a thickness of 1 mm were cut using wire electrical discharge machine and shown in figure 1. Load biased heating-cooling experiments under increasing stress magnitudes starting from 100 MPa and increasing by 100 MPa after each cycle with a heating-cooling rate of 10 °C min⁻¹ were conducted till fracture in order to compare the shape memory characteristics such as actuation strain, irrecoverable strain, TTs and thermal hysteresis.

Additionally, a JEOL transmission electron microscope (TEM) was utilized to investigate the twinning, precipitation and dislocation structures before and after the applied aforementioned processes. TEM samples were prepared using a focused ion beam equipment for thinning the samples down to 10–20 nm.

3. Experimental results

3.1. DSC analysis

DSC results of HE, HE-A, S and S-CR-A samples are shown in figure 2. The TTs were drawn from the DSC curves and are summarized in table 1. DSC results of HE and HE-A samples were shown in our previous study [16], however, the DSC results which were obtained from all samples were re-plotted in one graphic and all the TTs which were drawn from the DSC curves were re-tabulated for better comparison.

Three cycles were run to determine the shift in the TTs. TTs of the solutionized sample were found to be the highest. DSC experiment was also run on the cold rolled sample; however, no visible transformation was detected since the TTs were shifted to very low temperatures. This result is consistent with the previous studies for highly deformed NiTi binary alloys [19, 21, 25]. Aging after cold rolling increased the TTs to higher temperatures such that A_s, A_f and M_s temperatures were determined and higher than that of the TTs of the solutionized sample. On the other hand, it was not possible to detect M_f temperature of the S-CR-A sample since the finish part of the martensitic transformation curve is not very well delineated. Additionally, hot extrusion also led to a decrease in the TTs since noticeable deformation was applied to the alloy during the extrusion process. After aging heat treatment of the hot extruded sample, TTs again increased to higher levels which were previously shown in the literature [11]. Additionally, aging after hot extrusion and cold rolling with subsequent aging after solutionizing heat treatment led to observe stable TTs starting from the second cycle due to the formation of precipitates via aging and dislocation formation via cold rolling. As stated in the literature, the TTs of all the samples can be stabilized as the number of cycles increases [24]. However, the number of cycles was kept as three in this study to see the direct effect of aging and cold rolling processes on the stability of the TTs of the ternary alloy.

3.2. Isobaric heating-cooling experiments

Isobaric heating-cooling experiments were performed, during which the samples were held under constant tensile stress while they were cooled and heated once at a rate of 10 °C min⁻¹. The stress magnitude was increased by 100 MPa till the fracture was observed for all samples while the samples were kept in the austenitic state. Figure 3 demonstrates how the irrecoverable and actuation strain values as well as the martensite start (M_s) temperature and thermal hysteresis were determined from a single thermal cycle. Figures 4(a) and (b) exhibit the comparison of thermal
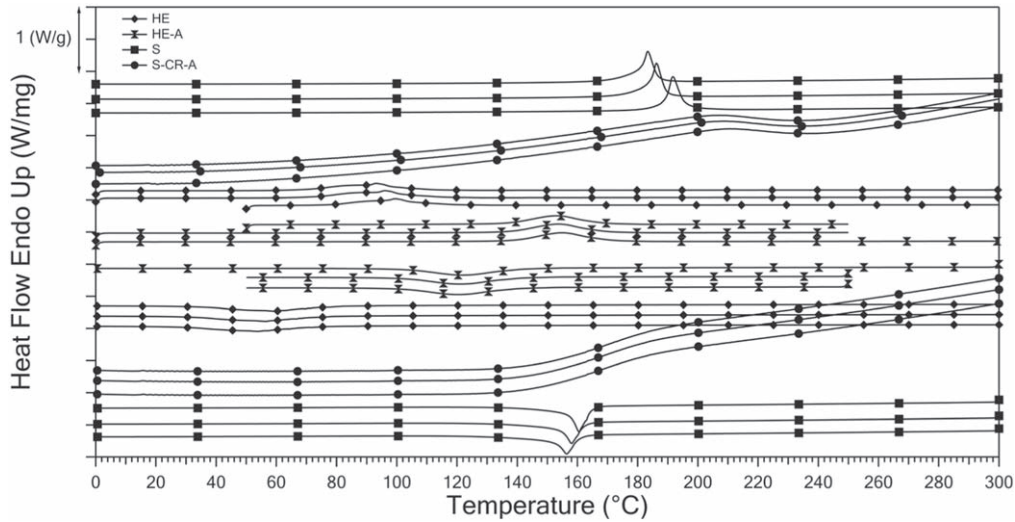
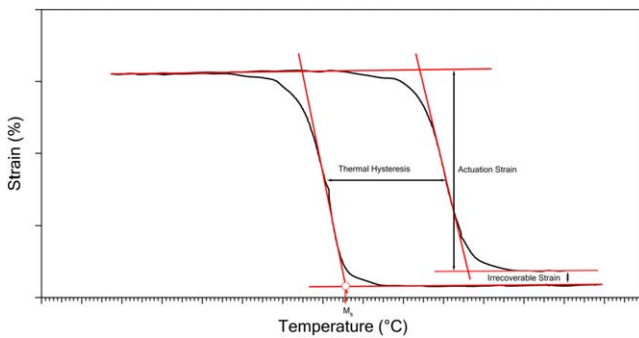**Figure 2.** DSC curves of the HE [16], HE-A [16], S, S-CR-A samples.

Figure 3. Schematic illustration which shows how to find out the M_s, thermal hysteresis, actuation and irrecoverable strain magnitudes from strain versus temperature curves.

Table 1. TTs which were drawn from the DSC curves in figure 2.

Sample	Cycle	Transformation temperatures (°C)			
		M_f	M_s	A_s	A_f
HE [16]	1	33.2	79.7	77.3	109.9
	2	30.2	78.2	70.4	106.5
	3	27	75.1	67	103.6
HE-A [16]	1	100.9	142	137.7	171.3
	2	99.9	141.3	136.4	168.9
	3	99.2	139.8	135.4	168.3
S	1	155.9	165.3	188.4	196.6
	2	153.3	163.1	180.8	190.6
	3	152.4	161.7	178.4	186.9
S-CR-A	1	—	187.5	85.1	244.5
	2	—	186.4	86	242.7
	3	—	185	85.1	241.9

function of applied stress. Additionally, M_s temperatures which were drawn from the strain versus temperatures graphs are presented in figure 6 to show the shift with the increasing stress magnitudes for all samples. The slopes which are representing $d\sigma/dT$ ratio were given on the same figure. Lastly, the evolution of the thermal hysteresis with the applied stress levels for all samples can be seen in figure 7. It should be noted that, the isobaric cooling-heating experiments of hot extruded and hot extruded with aging processed $Ni_{50.3}Ti_{29.7}Hf_{20}$ alloy were shown previously in the literature [11]. On the other hand, the transformation properties of SMAs may differ from batch to batch due to very small deviations in the composition, therefore, the cooling-heating under stress experiments were also conducted on the batch which was used in this study and the results are presented below for comparison.

The main observations from figures 4 and 5 can be summarized as:

(1) HE-A and S-CR-A samples fractured under the stress level of 700 MPa without showing noticeable irrecoverable strain levels. On the other hand, HE and S samples fractured under 600 MPa and 400 MPa during cooling step, respectively. Therefore, thermo-mechanical treatments such as rolling and aging increased the fracture strength of the alloy which are also experienced in previous studies conducted on binary NiTi [22, 23, 26].

(2) The actuation strain values increased with the increase of the stress magnitude for all samples. Additionally, the actuation strain values under all stress levels of the S-CR-A sample were determined to be very much lower than that of the other samples. These observations are consistent with the results which were observed in the cooling-heating under increasing constant stress experiments of binary NiTi alloy [23].

(3) Only irrecoverable strain magnitudes of the HE sample were noticeable after 200 MPa.

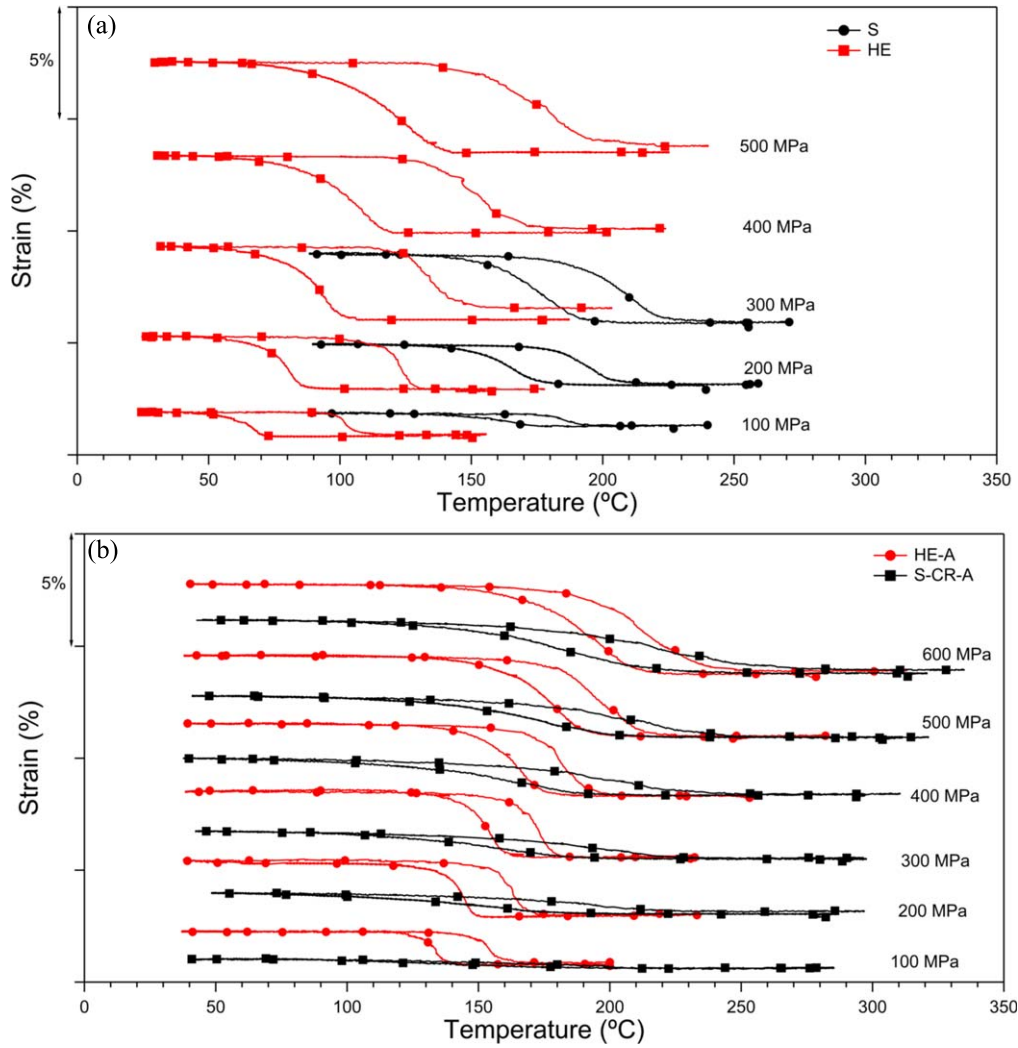cycling response of the HE and S samples and HE-A and S-CR-A samples under different stress levels, respectively. Actuation and irrecoverable strain magnitudes extracted from the strain-temperature curves are shown in figure 5 as a

Figure 4. The comparison of strain versus temperature curves obtained from heating-cooling cycles under different stress levels of (a) solutionized versus hot extruded samples (b) hot extruded and aged versus solutionized, cold rolled and aged samples.

(4) The undercooling magnitudes of S-CR-A sample which can be interpreted with the slope of the cooling curves of the strain versus temperature diagrams were very much higher than that of the other samples.

Figure 6 shows the dependence of M_s temperature with the applied stress magnitudes. As the temperature increases, the stress necessary to induce martensite which is called as σ_{SIM} increases as well. This behavior is the inverse temperature dependence of yield strength behavior of many metallic materials. In other terms, the stress magnitude for the yield of conventional metallic materials decreases as the temperature increases. σ_{SIM} depends on temperature with a positive slope according to the modified Clasius–Clapeyron (CC) relation. CC relation is [26, 27]:

$$\frac{d\sigma}{dT} = -\frac{\Delta H}{T_0 \varepsilon_{act}}$$

ΔH and T_0 are the transformation enthalpy and the chemical equilibrium temperature, respectively and ε_{act} is the actuation or transformation strain which is the difference in

between the total strain and the irrecoverable strain values. T_0 strongly depends on chemistry of the alloy. Since the alloy is the same, T_o can be accepted as constant for all the samples. The variables in CC equation are the transformation enthalpy and strain magnitudes and these values affect the slope of the curves, in other terms the ratio of $\frac{d\sigma}{dT}$. The slopes of HE, HE-A, S and S-CR-A samples were found as 5.8 MPa °C^{-1}, 6.8 MPa °C^{-1}, 8.6 MPa °C^{-1} and 11 MPa °C^{-1}, respectively. The slope magnitude increased steeply with the application of rolling with subsequent aging treatment after solutionizing heat treatment. The stability of the parameters in CC relation actually dictates the stability of the shape memory properties [24]. The rationale behind the differences between the slope magnitudes will be explained in the next section.

Figure 7 represents the thermal hysteresis response of all the samples with the increase of stress. The thermal hysteresis magnitudes of HE and S samples increased as the applied stress increased. However, there was no noticeable change in the thermal hysteresis magnitudes of HE-A and especially S-CR-A samples up to 500 MPa under increasing stress magnitude.

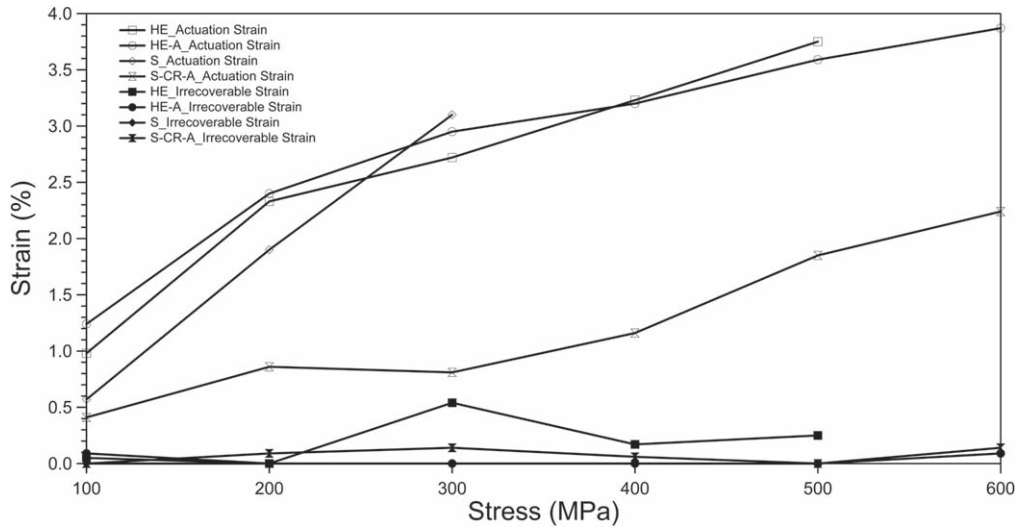**Figure 5.** The comparison of irrecoverable and actuation strain magnitudes with respect to the applied stress level for all samples.
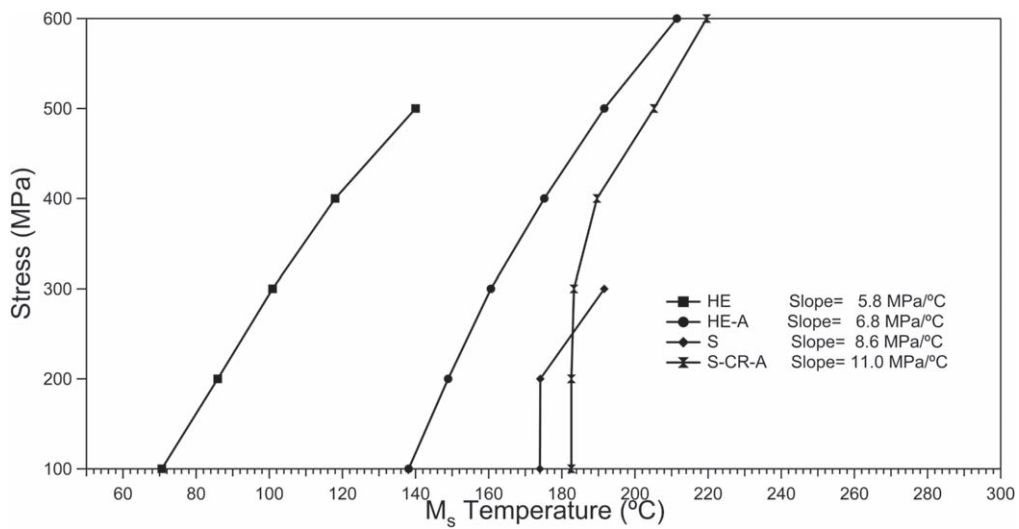

Figure 6. The comparison of M_s temperatures which were drawn from heating-cooling cycles under different stress levels of all samples.
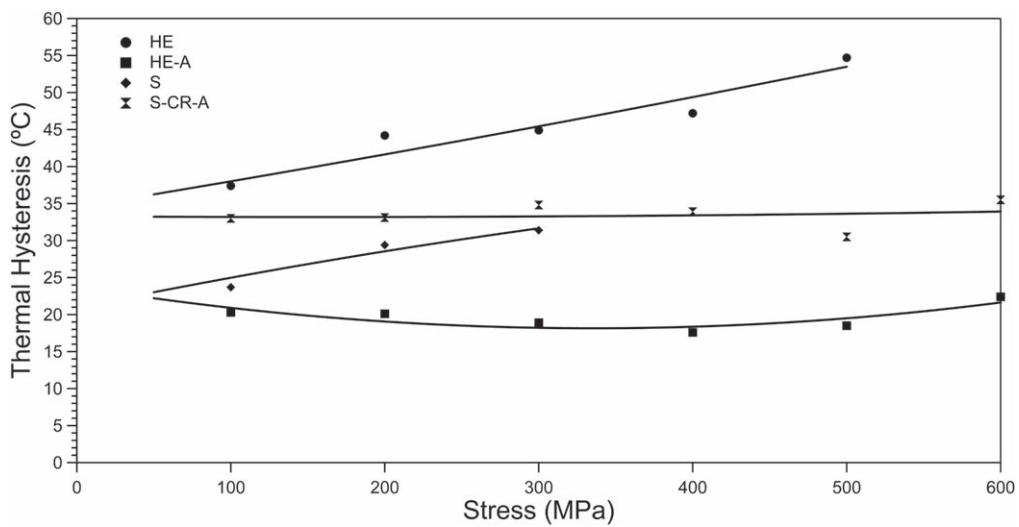

Figure 7. The comparison of thermal hysteresis values which were drawn from the heating-cooling cycles under different stress levels of all samples.

3.3. Microstructural evolution

TEM images which were taken from HE and S samples are presented in figure 8. Additionally, TEM images of HE-A and S-CR-A samples are presented in figure 9. Figure 8 (a) shows the unique microstructure which is called as herring-bone morphology in the literature [28]. Twinned lamellae structures and the junction planes between the twin variants are demonstrated by full lines and dashed line, respectively. On the other hand, solutionized sample shows only martensitic plates.

After aging of the hot extruded sample, high volume fraction of nano-sized precipitation formation is observable and the distribution of these precipitates is shown in figure 9(a). Figure 9(b) is representative of the microstructure of solutionized, cold rolled and aged sample. As can be seen in the 1st circled area, the boundaries of the martensitic plates are not very well delineated due to the dislocation density increase via cold rolling process. The 2nd circled area represents the very fine nano-precipitates which were formed after aging process.

4. Discussion of the results

The main goal of this study was to compare the actuation behavior of the HE, HE-A, S and S-CR-A treated $Ni_{50.3}Ti_{29.7}Hf_{20}$ alloy to eliminate the hot extrusion step for easier processing since extruding the hard to deform NiTiHf materials at relatively higher temperatures generally requires expensive and complicated tools.

The TTs without applying stress and with applying stress and actuation-irrecoverable strain values with cooling-heating under increasing stress magnitudes together with the microstructural evolution via following different thermo-mechanical processes were revealed. The rationales behind all the results which were shown in the previous section are explained in the subsections of this chapter.

4.1. The effect of thermo-mechanical treatments on the TTs

10% of cold rolling of the solutionized $Ni_{50.3}Ti_{29.7}Hf_{20}$ alloy sample showed no transformation peaks in DSC experiment due to the dislocation density increase with the rolling process. After aging the cold rolled sample at 550 °C for 3 h, the forward and reverse transformation peaks were observed, however, the aging treatment was still not enough to determine the martensite finish temperature. Cold rolling induces high amount of dislocation to the alloy and this led to martensite stabilization [22, 23]. On the other hand, aging treatment led to the formation of Ni-rich nano-precipitates such that the Ni concentration of the matrix decreased and the TT increased. Karaman group also revealed the annealing effect of thermal treatment after cold and warm rolling processes which led to an increase in TTs of near equiatomic $Ni_{50}Ti_{30}Hf_{20}$ alloy [17]. The aging treatment in this study may also anneal the sample but this might not be the main reason of
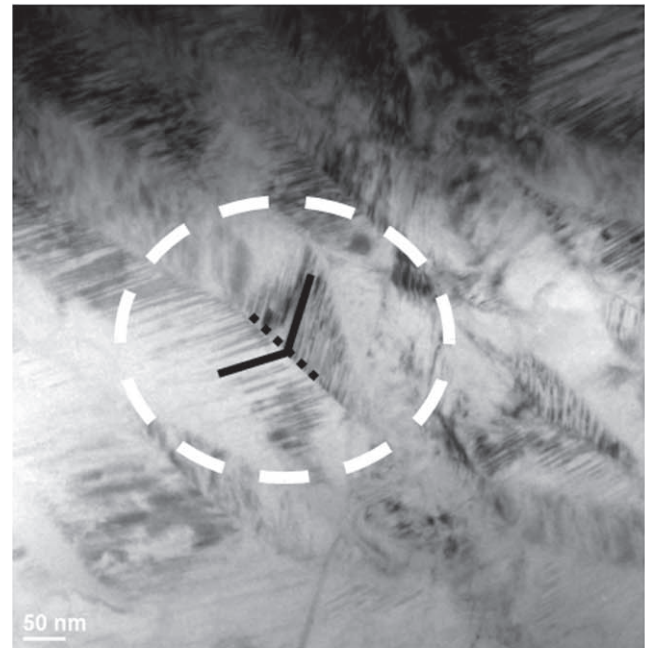
(a)
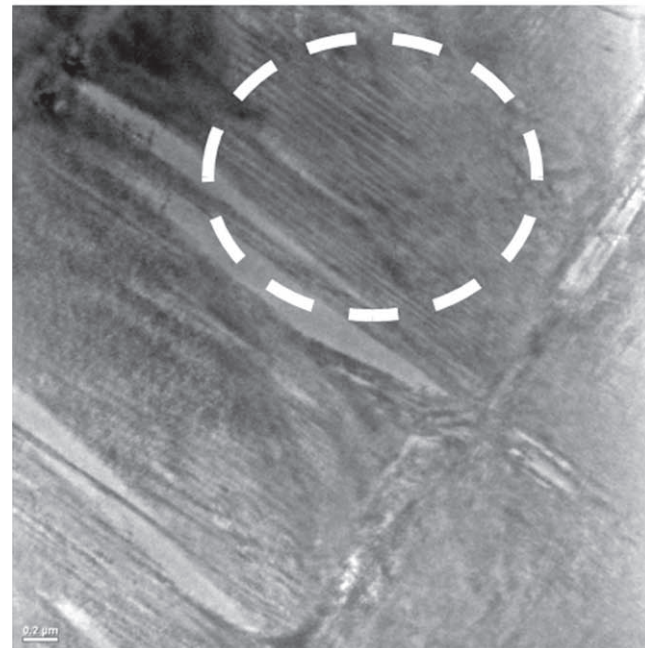
(b)

Figure 8. TEM images of (a) HE and (b) S Samples.

the increase in TTs since the martensite finish temperature of the S-CR-A sample was still not able to be determined.

Another intriguing finding is the observation of considerably higher TTs in the solutionized sample comparing with the TTs of the hot extruded sample. Although hot extrusion process was conducted at 900 °C, the TTs decreased considerably due to the refinement of the microstructure as it was shown in figure 8(a). The decrease in the TTs can be attributed to the very fine twin structure and the herring bone morphology. The aging treatment after hot extrusion process
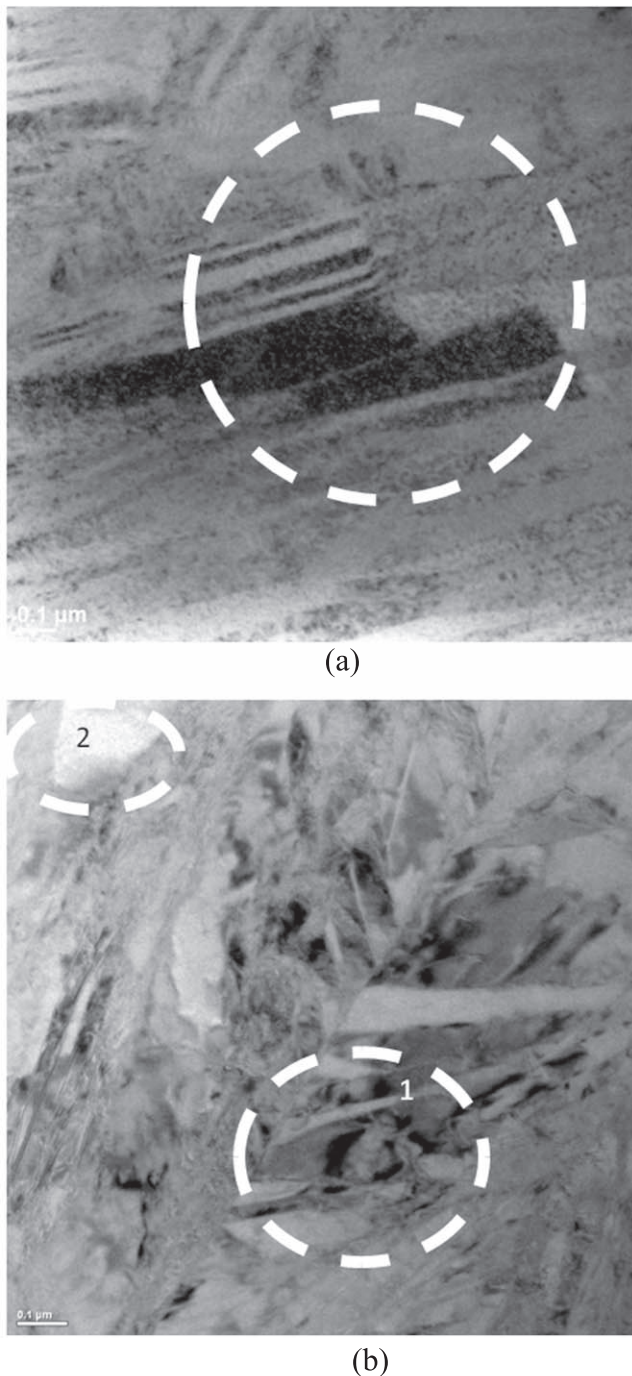
(a)

(b)

Figure 9. TEM images of (a) HE-A and (b) S-CR-A Samples.

increased the TTs due to precipitation formation and this mechanism has been already explained in the literature, extensively [11].

Additionally, the TTs of HE-A and S-CR-A samples were observed to be highly stable from the beginning of the thermal cycling as can be seen in table 1. Moreover, the thermal hysteresis of the S-CR-A sample which were obtained from the cooling-heating under constant stress experiments up to 500 MPa were more stable than that of the other samples due to the increase in the dislocation density and the precipitation formation.

4.2. The effect of thermo-mechanical treatments on the actuation and irrecoverable strain and thermal hysteresis

The effect of thermo-mechanical treatments on the dimensional stability of $Ni_{50.3}Ti_{29.7}Hf_{20}$ is one of the most important issues that should be discussed since dimensional stability is the main design criterion for actuator applications. Therefore, in this section the actuation and irrecoverable strain magnitudes which were gathered from all cooling-heating under constant stress experiments are discussed.

The actuation strain magnitudes of all thermo-mechanically treated samples increased as the applied stress levels were increased since the externally applied stress helped the formation of martensitic variant with the most favorable orientation which led to an increase in the external shape change. The actuation strain at each stress level for the S-CR-A sample were determined to be lower than that of the other samples due to the increase strength of the sample with cold deformation. The critical stress level to induce phase transformation in S-CR-A must be higher such that higher stress magnitudes should be necessary to achieve higher actuation strain levels. The same behavior was observed previously in ECAE processed NiTi binary alloy [26]. Moreover, cold rolling might induce texture to the NiTiHf alloy and this texture led to achieve less actuation strain values since it has been already known that cold drawn polycrystalline NiTi alloys exhibit a strong texture of [111] type at which the worst shape memory behavior is expected [29].

It was observed that the irrecoverable strain magnitudes of all the samples at each stress levels were found to be very low. Only 0.4% of irrecoverable strain was observed for HE sample under 300 MPa and then decreased down to lower values as the applied stress was increased since the sample might be further strengthened with the externally applied stresses. The HE-A and S-CR-A samples have been already strong due to nano-precipitate formation and inducing dislocation via cold rolling process. It is difficult to comment on the mechanical behavior of solutionized (S) sample since this sample showed early fracture, however S sample did not reveal any irrecoverable strain up to 300 MPa. Actually, these results are very well consistent with the results obtained from figure 6. Figure 6 shows the CC slopes of all samples. S-CR-A sample which revealed the lowest actuation strain showed the highest CC slope. Although CC slopes of the HE and HE-A samples differed they showed almost the same actuation strain magnitudes at each stress levels. This might be attributed to the formation of nano-precipitates which can enhance the phase transformation with the stress fields around the coherent precipitates.

Figure 7 presents the thermal hysteresis comparison of all the samples at each stress levels. It can be concluded from the graph that aging after hot extrusion and cold rolling with subsequent aging treatment after solutionizing enhance the stability of the thermal hysteresis of the alloy. The positive effect of aging on the cyclic stability of the NiTiHf alloys in terms of thermal hysteresis has been already shown and discussed in the literature [11, 14–16]. However, the enhancing effect of cold rolling with subsequent aging was shown in this

study and the stability of the thermal hysteresis of S-CR-A sample up to 500 MPa was more pronounced. Since the strength of HE-A and S-CR-A samples was increased with the precipitate and dislocation formation, the thermal hysteresis was not affected with the increase of the externally applied stress. Actually, the thermal hysteresis values of NiTi based alloys increase due to the increase in dislocation density with the increased stress magnitudes and with the number of cycles [26].

The thermal hysteresis values of HE-A sample and S-CR-A sample change between 20 °C–25 °C and 30 °C– 35 °C. The increase in the thermal hysteresis of the S and HE samples might be attributed to the increase in dislocation density with the increase in the applied stress. Additionally, the slopes of the cooling and heating curves of S-CR-A sample which were shown in figure 4(b) became shallow such that the forward and reverse transformations can be completed via applying more supercooling and superheating respectively due to the high dislocation density which hinders the martensitic transformation.

4.3. The effect of thermo-mechanical treatments on the microstructural evolution

TEM images in figures 8(a) and 9(a) reveal the microstructures of HE and HE-A samples. High volume of nano-precipitate formation was obtained after aging heat treatment and precipitate density was shown in figure 9(a). On the other hand, figure 8(a) reveals the very fine twin structure and herring bone morphology after hot extrusion process. Hot extrusion was conducted at 900 °C and it was not expected to refine the microstructure at this high deformation temperature but the percentage of the deformation which was 4 to 1 area reduction might lead to this refinement.

Figures 8(b) and 9(b) represent TEM images of S and S-CR-A samples. The characteristic martensitic structure was obtained after solutionizing treatment; however, cold rolling and aging led to an increase in dislocation density and nano-precipitate formation, respectively.

5. Summary and conclusions

In this study, the effect of thermo-mechanical treatments such as hot extrusion with subsequent aging and cold rolling with subsequent aging of solutionized $Ni_{50.3}Ti_{29.7}Hf_{20}$ alloy was investigated. The TTs, actuation and irrecoverable strain magnitudes and thermal hysteresis values of all thermo-mechanically treated samples were compared. The main findings and conclusions via analyzing the experimental results can be summarized as follows:

(1) The TTs can be stabilized with the number of cycles not only by hot extrusion with subsequent aging treatment but also by cold rolling with subsequent aging treatment of the solutionized alloy.

(2) It has been already proved in the literature that hot extrusion with subsequent aging treatment increases CC

slope of the Ni-rich NiTiHf alloys and in this study, the highest CC slope was achieved by cold rolling with subsequent aging treatment of solutionized $Ni_{50.3}Ti_{29.7}Hf_{20}$ alloy due to the increase in dislocation density and hence the strength of the alloy such that the dimensional and thermal hysteresis stability under increased stress levels were maintained. However, due to the increase in CC slope of the S-CR-A sample, the actuation strain values were less than that of the other samples.

(3) Cold rolling with subsequent aging of solutionized sample and hot extruded with aging processed sample showed very low irrecoverable strain magnitudes even at very high stress magnitudes in cooling-heating under stress experiments. Therefore, cold rolling and subsequent aging processes after solutionizing heat treatment can be an alternative thermo-mechanical treatment path to aging treatment after hot extrusion process. However, it should be noted that the actuation strain values of S-CR-A sample at each stress levels were found to be the lowest.

(4) The thermal hysteresis was not affected by the increased applied stress and the number of cycles after hot extrusion with subsequent aging of the alloy and cold rolling with subsequent aging treatment of the solutionized alloy.

(5) In the light of the experimental results, it can be concluded that hot extrusion is not a mandatory step to get improved resistance to plastic deformation. One can also follow a different thermo-mechanical route to achieve higher strength as well as better shape recovery properties in NiTiHf alloy. Hot extrusion is very useful in obtaining chemical and microstructural homogeneity but additional thermal and/or thermo-mechanical treatments can be the processing steps in enhancing the shape memory behavior of the alloy.

ORCID iDs

Benat Kockar https://orcid.org/0000-0001-8261-509X

References

[1] Ma J, Karaman I and Noebe R D 2010 High temperature shape memory alloys *Int. Mater. Rev.* **55** 257–315

[2] Meng X L, Cai W, Chen F and Zhao L C 2006 Effect of aging on martensitic transformation and microstructure in Ni-rich TiNiHf shape memory alloy *Scr. Mater.* **54** 1599–604

[3] Evirgen A, Karaman I, Noebe R D, Santamarta R and Pons J 2013 Effect of precipitation on the microstructure and the

shape memory response of the $Ni_{50.3}Ti_{29.7}Zr_{20}$ high temperature shape memory alloy *Scr. Mater.* **69** 354–7

[4] Lindquist P G and Wayman C M 1990 *Engineering Aspects of Shape Memory Alloys* ed T W Duerig *et al* (Boston, MA: Butterworth) p 58

[5] Patriarca L and Sehitoglu H 2015 High-temperature superelasticity of $Ni_{50.6}Ti_{24.4}Hf_{25.0}$ shape memory alloy *Scr. Mater.* **101** 12–5

[6] Evirgen A, Basner F, Karaman I, Noebe R D, Pons J and Santamarta R 2012 Effect of aging on the martensitic transformation characteristics of a Ni-rich NiTiHf high temperature shape memory alloy *Funct. Mater. Lett.* **5** 1250038

[7] Angst D R, Thoma P E and Kao M Y 1995 The effect of hafnium content on the transformation temperatures of $Ni_{49}Ti_{51-x}Hf_x$ Shape memory alloys *J. Phys.* IV **05** C8-747–52

[8] Santamarta R, Arroyave R, Pons J, Evirgen A, Karaman I, Karaca H E and Noebe R D 2013 TEM study of structural and microstructural characteristics of a precipitate phase in Ni-richNi–Ti–Hf and Ni–Ti–Zr shape memory alloys *Acta Mater.* **61** 6191–206

[9] Karaca H E, Acar E, Tobe H and Saghaian S M 2014 NiTiHf-based shape memory alloys *Mater. Sci. Technol.* **30** 1530–44

[10] Evirgen A, Karaman I, Santamarta R, Pons J and Noebe R D 2015 Microstructural characterization and shape memory characteristics of the $Ni_{50.3}Ti_{34.7}Hf_{15}$ shape memory alloy *Acta Mater.* **83** 48–60

[11] Karaca H E, Saghaian S G, Ded G, Tobe H, Basaran B, Maier H J, Noebe R D and Chumlyakov Y I 2013 Effects of nanoprecipitation on the shape memory and material properties of an Ni-rich NiTiHf high temperature shape memory alloy *Acta Mater.* **61** 7422- 7431

[12] Saghaian S M, Karaca H E, Souri M, Turabi A S and Noebe R D 2016 Tensile shape memory behavior of $Ni_{50.3}Ti_{29.7}Hf_{20}$ high temperature shape memory alloys *Mater. Des.* **101** 340–5

[13] Bigelow G S, Garg A, Padula S A II, Gaydosh D J and Noebe R D 2011 Load-biased shape memory and superelastic properties of a precipitation strengthened high-temperature $Ni_{50.3}Ti_{29.7}Hf_{20}$ alloy *Scr. Mater.* **64** 725–8

[14] Karakoc O, Hayrettin C, Bass M, Wang S J, Canadinc C, Mabe H J, Lagoudas D C and Karaman I 2017 Effects of upper cycle temperature on the actuation fatigue response of NiTiHf high temperature shape memory alloys *Acta Mater.* **138** 185–97

[15] Karakoc O, Hayrettin C, Canadinc D and Karaman I 2018 Role of applied stress level on the actuation fatigue behavior of NiTiHf high temperature shape memory alloys *Acta Mater.* **153** 156–68

[16] Saygili H H, Tugrul H O and Kockar B 2018 Effect of aging heat treatment on the high cycle fatigue life of $Ni_{50.3}Ti_{29.7}Hf_{20}$ high-temperature shape memory alloy *Shape Mem. Superelasticity* **5** 32–41

[17] Babacan N, Bilal M, Hayrettin C, Liu J, Benafan O and Karaman I 2018 Effects of cold and warm rolling on the shape memory response of $Ni_{50}Ti_{30}Hf_{20}$ high-temperature shape memory alloy *Acta Mater.* **157** 228–44

[18] Kockar B, Karaman I, Kim J I and Chumlyakov Y 2006 A method to enhance cyclic reversibility of NiTiHf high temperature shape memory alloys *Scr. Mater.* **54** 2203–8

[19] Frick C P, Ortega A M, Tyber J, Maksoundb A E M, Maier H J, Liu Y and Gall K 2005 Thermal processing of polycrystalline NiTi shape memory alloys *Mater. Sci. Eng.* A **405** 34–49

[20] Gall K, Tyber J, Wilkesanders G, Robertson S W, Ritchie R O and Maier H J 2008 Effect of microstructure on the fatigue of hot-rolled and cold-drawn NiTi shape memory alloys *Mater. Sci. Eng.* A **486** 389–403

[21] Treppmann D and Hornbogen E 1997 On the influence of thermomechanical treatments on shape memory alloys *J. Phys.* IV **7** 211–20

[22] Kockar B, Karaman I, Kulkarni A, Chumlyakov Y and Kireeva I V 2007 Effect of severe ausforming via equal channel angular extrusion on the shape memory response of a NiTi alloy *J. Nucl. Mater.* **361** 298–305

[23] Miller D A and Lagoudas D 2001 Influence of cold work and heat treatment on the shape memory effect and plastic strain development of NiTi *Mater. Sci. Eng.* A **308** 161–75

[24] Morgan N B and Friend C M 2001 A review of shape memory stability in NiTi alloys *J. Phys.* IV **11** 325–32

[25] Legresy J M, Prandi B and Raynaud G M 1991 Effects of cold-rolling and post-deformation annealing on the martensitic transformation of a TiNi shape memory alloy *J. Phys.* IV **1** 241–6

[26] Kockar B, Karaman I, KimJ I, Chumlyakov Y I, Sharp J and Yu (Mike) C J 2008 Thermomechanical cyclic response of an ultrafine-grained NiTi shape memory alloy *Acta Mater.* **56** 3630–46

[27] Liu Y and McCormick P G 1994 Thermodynamic analysis of the martensitic transformation in NiTi: I. Effect of heat treatment on transformation behaviour *Acta Metall. Mater.* **42** 2401–06

[28] Waitz T 2005 The self-accommodated morphology of martensite in nanocrystalline NiTi shape memory alloys *Acta Mater.* **53** 2273–83

[29] Gall K and Maier H J 2002 Cyclic deformation mechanisms in precipitated NiTi shape memory alloys *Acta Mater.* **50** 4643–57